

Early and
Mid-Holocene climate
in the tropical Pacific

Y. Luan et al.

Early and mid-Holocene climate in the tropical Pacific: seasonal cycle and interannual variability induced by insolation changes

Y. Luan^{1,2,3}, P. Braconnot², Y. Yu¹, W. Zheng¹, and O. Marti²

¹State Key Laboratory of Numerical Modeling for Atmospheric Sciences and Geophysical Fluid Dynamics (LASG), Institute of Atmospheric Physics (IAP), Beijing, China

²Laboratoire des Sciences du Climat et de l'Environnement (LSCE/IPSL), Unité mixte CEA-CNRS-UVSQ – UMR8212, Orme des Merisiers, Gif sur Yvette, France

³Graduate University of Chinese Academy of Sciences, Beijing, China

Received: 16 January 2012 – Accepted: 24 January 2012 – Published: 6 February 2012

Correspondence to: Y. Luan (yihua.luan@lsce.ipsl.fr)

Published by Copernicus Publications on behalf of the European Geosciences Union.

Title Page

Abstract

Introduction

Conclusions

References

Tables

Figures

⏪

⏩

◀

▶

Back

Close

Full Screen / Esc

Printer-friendly Version

Interactive Discussion



Abstract

Using a coupled atmosphere-ocean model we analyze the responses of the mean climate and interannual variations in the tropical Pacific to the changes in insolation during the early and middle Holocene, for which only the variations of Earth's orbital configuration are considered. Comparison of the early and mid-Holocene with pre-industrial climate shows that both the mean climate and the characteristics of the interannual variability are altered by the changes in insolation. In particular, there is a decrease of the annual mean SST, which is characterized by a "U" shape across the tropical Pacific. The changes of the SST seasonal cycle are consistent with the changes in insolation, with the SST amplitudes weakening in the tropics. However, the larger changes in seasonality are found in the eastern Pacific, where thermodynamics and dynamical processes strengthen the SST response. The cloud radiative forcing largely reduces the shortwave radiation in the western tropical Pacific in winter causing a zonally asymmetric heat flux response. Simulations also show that ENSO strengthens across the Holocene, as suggested by coral data or lake sediments. The role of the obliquity is examined by a sensitivity experiment and we find that the obliquity change affects the seasonal displacement of ITCZ related to strength of SST meridional gradients. However, the obliquity change has little effect on SST seasonal cycle and interannual variability in eastern tropical Pacific. The precession of the orbital parameter is more important in effecting the tropical climate.

1 Introduction

The El Niño-Southern Oscillation (ENSO) phenomenon is the most important manifestation of short-term climate variability resulting from air-sea interactions in the tropical Pacific (Philander, 1990). This coupled ocean-atmosphere mode impacts weather and climate patterns not only in Tropics but also in extra-Tropics, and is of vital importance for numerous countries (Ropelewski and Halpert, 1986; Lau and Nath, 2000; Wang et

CPD

8, 505–555, 2012

Early and Mid-Holocene climate in the tropical Pacific

Y. Luan et al.

Title Page

Abstract

Introduction

Conclusions

References

Tables

Figures



Back

Close

Full Screen / Esc

Printer-friendly Version

Interactive Discussion



al., 2000; Annamalai et al., 2007). El Niño events develop every 2 to 7 years at present. During these events the anomalous westerly wind and deep convection are shifted in the central equatorial Pacific Ocean and warm water invade the equatorial cold tongue (Wang, 1992). Warm ENSO events have their cold counterpart – La Niña events. They have opposite characteristics resembling to an enhancement of the normal conditions, with enhanced trade wind and SST gradients across the Pacific. Analysis of the instrumental records shows that each event has its own characteristics. They also show that ENSO frequency increased in the last years of the twenty century, with the maximum SST anomalies located in the middle of the basin but not at the east coast as in the traditional view (Latif et al., 1997; Kao and Yu, 2009; Kug et al., 2009; Yeh et al., 2009). These changes appear to be connected to shifts in mean climate, raising the possibility that ENSO might undergo discernible changes in response to anthropogenic driven warming. However, even though most climate model now reproduces ENSO variability, there is no agreement on its future evolution when inferred from climate projections (IPCC, 2007). Different models project a wide range of responses from weakened to strengthened ENSO (e.g. van Oldenborgh et al., 2005; Guilyardi et al., 2006; Merryfield, 2006). Changes in the mean state of the tropics are also uncertain, with models simulating responses ranging from “El Niño-like” to “La Niña-like” changes in tropical Pacific zonal SST gradients (e.g. Collins et al., 2005; Merryfield, 2006). There is thus a great need to further understand ENSO and how it is affected by changes in the background climate state. The record of past climate conditions provides a unique opportunity to achieve these goals.

Both proxy reconstructions in the Pacific Basin (e.g. Rodbell et al., 1999; Moy et al., 2002) and coupled model simulations (Hewitt and Mitchell, 1998; Otto-Bliesner, 1999; Bush, 1999; Clement et al., 1999, 2000; Liu et al., 1999, 2000) indicate that significant changes in ENSO characteristics took place in the Holocene. The main forcing of the ENSO evolution during the Holocene is the changes in insolation seasonal cycle due to precession and obliquity. During the Holocene, the change in the timing of perihelion from boreal winter to boreal summer resulted in an increased Northern

Early and Mid-Holocene climate in the tropical Pacific

Y. Luan et al.

Title Page

Abstract

Introduction

Conclusions

References

Tables

Figures



Back

Close

Full Screen / Esc

Printer-friendly Version

Interactive Discussion



Hemisphere (NH) seasonal cycle, while reducing the strength of Southern Hemisphere (SH) seasonality (Berger, 1978). As modern ENSO is observed to be strongly phase-locked to the seasonal cycle (Wang and Picaut, 2004), it might be expected that such a change in the seasonal cycle would alter the behavior of ENSO in the Holocene. Interannual variability of coral oxygen isotope and Sr/Ca ratios at ENSO periods is found to be weaker in mid-Holocene coral than in modern coral from the same site, implying reduced ENSO amplitude (Tudhope et al., 2001). Rodbell et al. (1999) using a high resolution 15 000 year record of lake deposits in Ecuador suggests that strong ENSO events became established only from 5000 years ago. McGregor and Gagan (2004) reports ENSO amplitude reduction of 15 % in fossil coral records from a northern Papua New Guinea site using a measure based on the average coral isotopic anomaly for El Niño events over a threshold. In addition, several high-resolution records suggest reduced activity of the ENSO (e.g. McGlone et al., 1992). Wen et al. (2007) gave an overview about the progress of the paleo-ENSO studies. Coupled atmosphere-ocean models were used to explore the mechanism of ENSO changes in Holocene (Table 1). They pointed out that insolation change is the main reason to reduce the amplitude of the interannual variability through the influence of extra-tropical monsoon (Liu et al., 2000, 2003) and Bjerknes feedback (Clement et al., 2000, 2001). During the early to mid-Holocene monsoon was enhanced in several regions (Wright et al., 1993; Liu et al., 2003) due to the orbital configuration; the seasonal cycle of the incoming solar radiation at the top of the atmosphere was enhanced in the northern Hemisphere. Other mechanisms also appear to be at work. Chiang et al. (2009) indicated that the mid-Holocene ENSO reduction was caused by Pacific-wide climate changes to mid-Holocene orbital conditions. They suggested that the mid-Holocene ENSO changes are not driven by mean-state changes in the tropical Pacific but rather from mid-Holocene insolation applied outside of the tropical Pacific. Rodbell (1999) suggested that the reduced SST gradient between the western Pacific warm pool and the eastern Pacific cold tongue mainly damp the ENSO development in Holocene epochs. Results from an ensemble of mid-Holocene simulations run with different climate models as part of the second

Early and Mid-Holocene climate in the tropical Pacific

Y. Luan et al.

[Title Page](#)[Abstract](#)[Introduction](#)[Conclusions](#)[References](#)[Tables](#)[Figures](#)[Back](#)[Close](#)[Full Screen / Esc](#)[Printer-friendly Version](#)[Interactive Discussion](#)

phase of Paleoclimate Modeling Intercomparison Project (PMIP2) also show a reduced ENSO amplitudes at 6 ka than at present (Zheng et al., 2008). Those hypotheses mentioned above are not fully supported in PMIP simulations.

Above all, most previous studies using coupled models focused on the ENSO characteristics in the mid-Holocene. Only a few studies considered the changes in mean state and interannual variability in the early Holocene and compared the early Holocene with the mid-Holocene, even though results from transient simulations become available (Timmermann et al., 2007). The mean state of Holocene tropical Pacific SSTs has been reconstructed from Palaeoclimate records including oxygen isotope ratios and Mg/Ca ratios (e.g. Koutavas et al., 2002; Stott et al., 2004; Lea et al., 2006; Sandweiss et al., 1996). Climate reconstructions based on different proxy indicators disagree widely on the changes of annual mean SST in tropical Pacific. In the mid-Holocene, some reconstructions indicate that SST warm both in the western Pacific (Stott et al., 2004; McGlone et al., 1992) and in the eastern Pacific (Sandweiss et al., 1996). However, Koutavas et al. (2002) indicates SST was cold in the east Pacific compared to present day. Stott et al. (2004) used oxygen and Mg/Ca data from foraminifers retrieved from three sediment cores in the western tropical Pacific show that there is a decrease in SST of 0.5 °C over the past 10 000 yr. There is also evidence that the western equatorial Pacific was more saline in the mid-Holocene according to reconstructions from oxygen isotope ratios in coral (Gagan et al., 1998; Tudhope et al., 2001) and marine sediments (Stott et al., 2004), implying decreased precipitation or increased evaporation.

Braconnot et al. (2011) has used the climate system model IPSL_CM4 to look at the relative influence of the orbitally-driven changes and a fresh water flux in the North Atlantic on the climate seasonal cycle and interannual variability changes. They show that the insolation forcing affects both the tropical Pacific SST seasonal cycle and ENSO characteristics and that the resulting changes have a larger magnitude than that the changes induced by a fresh water flux release in the north Atlantic. They also discussed the fact that Holocene SST changes are dominated by changes in seasonality

Early and Mid-Holocene climate in the tropical Pacific

Y. Luan et al.

Title Page

Abstract

Introduction

Conclusions

References

Tables

Figures



Back

Close

Full Screen / Esc

Printer-friendly Version

Interactive Discussion



in most of the tropical Pacific. However, the processes by which the insolation forcing affects climate in the tropical Pacific need further exploration. In this study, we use the same set of simulations to analyze in more depth the changes in mean seasonal cycle and interannual variability changes induced by insolation changes. In particular we link the changes in SST and in ocean stratification to the insolation forcing, considering the surface fluxes. We also highlight some of the differences between EH and MH, considering the phase relationship between the development of the ENSO events and the seasonal evolution of the background mean state. The relative roles of the obliquity and precession are further explored considering a sensitivity experiment to the early Holocene obliquity. The paper is organized as follows: climate simulations and analyses are first described in Sect. 2. Sections 3 and 4 analyze the characteristics of the pre-industrial climate and the simulated changes for the early and mid-Holocene. The role of the obliquity is discussed in Sect. 5. Discussion and conclusions are presented in Sect. 6.

2 Climate simulations and analyses

2.1 Model description

We consider the simulations of the pre-industrial, the mid-Holocene (6 ka BP) and the early Holocene (9.5 ka BP) discussed in Marzin and Braconnot (2009) and Braconnot et al. (2011). These simulations were run using the coupled ocean-atmosphere general circulation model IPSL_CM4 (Marti et al., 2010). The version is the same with the one used for CMIP3 experiments (Meehl et al., 2007) that served as a basis for the Fourth IPCC Assessment Report (IPCC AR4) (Solomon et al., 2007). It contains four components. The atmospheric component is the grid point atmospheric general circulation model LMDZ (Hourdin et al., 2006) developed at Laboratoire de Météorologie Dynamique (LMD, France). It has a resolution of 96 grid points in longitude, 72 grid points in latitude and 19 vertical levels. The oceanic component is the

CPD

8, 505–555, 2012

Early and Mid-Holocene climate in the tropical Pacific

Y. Luan et al.

Title Page

Abstract

Introduction

Conclusions

References

Tables

Figures

⏪

⏩

◀

▶

Back

Close

Full Screen / Esc

Printer-friendly Version

Interactive Discussion



**Early and
Mid-Holocene climate
in the tropical Pacific**Y. Luan et al.

[Title Page](#)[Abstract](#)[Introduction](#)[Conclusions](#)[References](#)[Tables](#)[Figures](#)[Back](#)[Close](#)[Full Screen / Esc](#)[Printer-friendly Version](#)[Interactive Discussion](#)

oceanic general circulation model ORCA (Madec et al., 1998) developed at the Laboratoire d'Océanographie et du Climat (LOCEAN, France) with the resolution of 182 points in longitude, 149 points in latitude and 31 vertical levels. The ORCA model uses the OPA system for ocean dynamics. The land surface scheme is ORCHIDEE (Krinner et al., 2005) and only the thermodynamic and hydrological components are active in the simulation here. A river runoff scheme is used to close the fresh water budget between land and ocean. The sea-ice model LIM (Fichefet and Maqueda, 1997) is included in the ocean model to compute sea ice dynamic and thermodynamic. The ocean and atmosphere are coupled using the OASIS coupler (Terray et al., 1995) developed at CERFACS (France) once a day and there is no flux correction.

2.2 Experiments

The PI simulation (pre-industrial period: 0 ka BP) was carried out using modern orbital parameters, vegetation coverage, continental ice sheets and topography. The greenhouse gases were set to pre-industrial (around 1750) concentrations (i.e. CO₂: 280 ppm, CH₄: 760 ppb, N₂O: 270 ppb) (<http://pmip2.lsce.ipsl.fr/>). The simulation is more than 1000 years long and is stable (the global surface temperature trend is less than 0.02 K/century, Marti et al., 2010). The initial state of the ocean is rest, with temperature and salinity prescribed to Levitus's (1983) climatology. A 1st January of the ERA15 reanalysis from ECMWF is for the initial state of atmosphere. The soil model is initialized with a water content of 300 mm, and no snow cover (Marzin and Braconnot, 2009; Marti et al., 2010). The model was first adjusted for several centuries before running the PI simulation.

The MH simulation (mid-Holocene: 6 ka BP) and EH simulation (early Holocene: 9.5 ka BP) were forced with the same continental ice sheets and topography as in the PI simulation but account for the changes in the Earth's orbital parameters (Marzin and Braconnot, 2009). The orbital parameters were prescribed from Berger (1978). The MH simulation corresponds to the PMIP2 simulation and also accounts for small changes in greenhouse gases following PMIP2 recommendations (CO₂: 280 ppm,

CH₄: 650 ppb and N₂O: 270 ppb) (Braconnot et al., 2007, <http://pmip2.lsce.ipsl.fr/>). The global energetic of the model is only slightly affected by the changes in orbital parameters; the annual mean change of the insolation is negligible (0.011 Wm⁻²) when averaged globally. It induces, however, a more than 30 Wm⁻² change in seasonal insolation. Simulations for the 6 and 9.5 kaBP climates are 650 and 500 years long, respectively. The initial state is the same as the one of the PI simulation. The model adjusts in 60 to 100 years to the new boundary conditions.

All simulations were run long enough to be representative of an equilibrium climate. For the analysis, we use monthly time series from the last part of the simulations where the climate characteristic is stable. This corresponds to 770 years for the PI simulation and varies from 219 to 370 years respectively for the EH and MH simulations as discussed in Braconnot et al. (2011).

3 Characteristics of the pre-industrial climate

3.1 Large scale features and seasonality

The coupled model IPSL_CM4 captures successfully the large scale features of the tropical circulation (Braconnot et al., 2007a,b; Marti et al., 2010). The annual mean large-scale distribution of SST is produced well, such as the warm pool in the western Pacific and the equatorial cold tongue in the eastern Pacific compared to the HadiSST reanalysis data (Rayner et al., 2003) (Fig. 1). But the equatorial cold tongue is too equatorially confined, and extends too far west into the western Pacific. This leads to a westward shift and an erosion of the warm pool. These biases are part of the systematic biases found in this class of non-flux-corrected GCMs (Latif et al., 2001) and are present in most of the PMIP2 simulations (Zheng et al., 2008). It is not directly associated with the insufficient resolution, for these biases also exist in the higher resolution model (Marti et al., 2010). In the tropical Pacific, the east-west SST gradient is correctly represented, with an exception near the Chile coast. There is a warm bias

Early and Mid-Holocene climate in the tropical Pacific

Y. Luan et al.

[Title Page](#)[Abstract](#)[Introduction](#)[Conclusions](#)[References](#)[Tables](#)[Figures](#)[Back](#)[Close](#)[Full Screen / Esc](#)[Printer-friendly Version](#)[Interactive Discussion](#)

along the coast of Peru and Chile. It results from the combination of insufficient wind along South America, the misrepresentation of cloud cover and the presence of a too developed double ITCZ structure in the eastern Pacific. The structure of the South Pacific Convergence Zone (SPCZ) is too zonal and penetrates too far toward the east Pacific (Marti et al., 2010), associated with excessive precipitation over much of the tropics. The pattern of precipitation is consistent with the temperature field (Braconnot et al., 2007a,b). Along the equator, the east-west gradient of wind stress is too strong, with a maximum near 160° W not well represented, and too strong eastward winds over the warm pool (Marti et al., 2010).

The CMIP3 models have errors in the tropical Pacific seasonal cycle; both in SST and wind, such as many models exhibit an overly strong seasonal cycle in the east Pacific or a spurious semi-annual cycle (Guilyardi et al., 2009). The seasonal cycle in the east Pacific in IPSL_CM4 is quite well represented compared to the other CMIP3 models, both in phase and amplitude (Marti et al., 2010). The annual cycle of sea surface temperature (SST) simulated for pre-industrial period in the eastern equatorial Pacific is consistent with the observation, but its phase is delayed about one month (Braconnot et al., 2011). The SST variability extends correctly from the east; however, its westward extension is slightly underestimated. The amplitude of the annual cycle (difference between maximum and minimum SST values) is also slightly weaker than observed.

3.2 ENSO characteristics

The IPSL_CM4 model simulates a larger variability and higher frequency than observed (about 2.7 years vs. 4–5 years in observations, Zheng et al., 2008). The ENSO amplitude is about right but the processes of damping ENSO in the model are too weak (Guilyardi et al., 2009). The model's tropical and ENSO simulations have consistently been ranked among the world's top GCMs in different comparisons with other CMIP3 simulations (van Oldenborgh et al., 2005; Guilyardi, 2006; Reichler and Kim, 2008).

CPD

8, 505–555, 2012

Early and Mid-Holocene climate in the tropical Pacific

Y. Luan et al.

Title Page

Abstract

Introduction

Conclusions

References

Tables

Figures



Back

Close

Full Screen / Esc

Printer-friendly Version

Interactive Discussion



**Early and
Mid-Holocene climate
in the tropical Pacific**Y. Luan et al.

[Title Page](#)[Abstract](#)[Introduction](#)[Conclusions](#)[References](#)[Tables](#)[Figures](#)[Back](#)[Close](#)[Full Screen / Esc](#)[Printer-friendly Version](#)[Interactive Discussion](#)

In order to analyze the changes of tropical Pacific interannual variability, we selected the typical El Niño and La Niña events from each simulation and observed data (HadiSST data from 1870 to 2003 yr). Firstly, the December-January-February (DJF) average of Niño3 index was calculated because it is a classical indicator of ENSO variability. Secondly, we carried out composite analysis for El Niño and La Niña events by using 1.2 times of standard deviation (1.2σ) as a criterion. In other words, if the DJF SST anomaly is larger (smaller) than $\pm 1.2\sigma$ in a given year, this year is selected for composite analysis. Large interannual variability of tropical Pacific SSTs in the EH and MH simulations is found in the middle and eastern tropical Pacific (Braconnot et al., 2011). Composites of all El Niño (La Niña) years for each period are used in the study. We only discuss in the following robust features. Details of the statistical analyses can be found in Braconnot et al. (2011).

Figure 2 shows the evolution of SST, precipitation and wind stress anomalies during El Niño years in the PI simulation, considering every two months from June preceding the peak of the event to the following April. This figure also compares the evolution of SST in the PI simulation with that in HadiSST data. El Niño onset occurs from May in the eastern part of the basin as observed. It is associated to a convergence of wind over the warm SST anomalies, as well as increased precipitation along the equator and decreased precipitation on both sides of the equator. Then the convergent wind stress becomes stronger and damps the oceanic upwelling in the middle and eastern tropical Pacific. The positive SST anomalies intensify reaching its peaking anomaly at the end of the El Niño year. The enhancement of precipitation anomaly occurs in the central and eastern Pacific (Fig. 2). The positive SST anomalies decrease after the El Niño year. The model reproduces this overall feature, but its spatial structure extends too far to the west and is too confined around the equator. No clear relationship is found between this bias and the characteristics of the model mean state bias in the equatorial Pacific. Leloup et al. (2008) have shown that this bias is mainly related to a misrepresentation of both El Niño and La Niña termination phases for most of the CMIP3 simulations. Guilyardi (2006), however, suggested that this classical bias of

coupled models is related to too strong mean zonal wind stress. In the observation, ENSO maximum amplitude occurs in the central-eastern Pacific. But the standard deviation of air temperature increases from the western Pacific to the eastern Pacific Ocean (AchutaRao and Sperber, 2006). The SST anomalies (SSTA) averaged over the Niño3 or Niño3.4 regions are then usually used to describe ENSO. IPSL_CM4 model simulates the maximum ENSO amplitude in the same area as the observations, even though the maximum is too strong in the Niño3.4 region (Fig. 2).

4 Simulated changes for the early and mid-Holocene

4.1 Changes in insolation

During the early and mid-Holocene, changes of insolation due to slow variations of the Earth's orbital parameters are the major drivers of climate variability. Precession and obliquity are the two parameters that shape the insolation forcing over the Holocene. Because of the precession, the summer solstice was close to the perihelion during the Early Holocene period (Marzin and Braconnot, 2009). Figure 3 shows the incoming solar radiation (Wm^{-2}) at the top of the atmosphere. As a consequence of precession, which shifts the timing of perihelion from boreal winter to boreal summer, the early and mid-Holocene were characterized by an enhanced seasonal cycle in the Northern Hemisphere (NH), while reduced seasonality in the Southern Hemisphere (SH) (Fig. 3b and d). Along the equator (averaged from $5^{\circ}S$ to $5^{\circ}N$ and removed annual mean), insolation is uniform and exhibits a semi-annual cycle with two maxima respectively in spring and autumn in the PI simulation (Fig. 3c). In the early Holocene, insolation is amplified by almost $30 Wm^{-2}$ during boreal summer and the maximum and minimum changes are in phase with the summer and winter solstices. The superposition of this annual mean cycle with the semi-annual cycle damps the boreal winter insolation forcing and strengthens the boreal summer insolation and the autumn maximum. A similar pattern is found for the mid-Holocene, with a maximum amplification of about

Early and Mid-Holocene climate in the tropical Pacific

Y. Luan et al.

[Title Page](#)[Abstract](#)[Introduction](#)[Conclusions](#)[References](#)[Tables](#)[Figures](#)[Back](#)[Close](#)[Full Screen / Esc](#)[Printer-friendly Version](#)[Interactive Discussion](#)

25 Wm^{-2} . It is slightly reduced compared to 9.5 ka BP, and it lags by about one month the 9.5 ka BP signal (Fig. 3c). Because of the lengths of the seasons are altered by the precession variations, the calendar we used for monthly average have a slight effect on the study (Joussaume and Braconnot, 1997). But it does not change the major conclusion.

4.2 Impact of orbital forcing on the surface fluxes

We present the changes of the annual mean surface radiative fluxes in Table 2. Surface radiative fluxes include the net solar radiation (SW, positive downward), the net long-wave radiation (LW, positive downward), the latent heat flux (LE, positive downward), the sensible heat flux (Hs, positive downward), and the net radiative flux (surface budget = SW + LW + LE + HS, positive downward). In the PI simulation, as in the modern climate, the annual mean net radiative flux is much larger in eastern Pacific where the thermocline is shallower than in the western Pacific (Table 2) stressing that the dynamical cooling resulting from zonal and meridional ocean heat transports plays a large role in these regions to balance the surface fluxes (Clement et al., 1996). As shown in Table 2, the net solar radiation in the two regions is mainly balanced by long wave and latent heat fluxes. However, the latent heat is more efficient over the warm water of the warm pool region. The difference in cloud cover and SST across the Pacific also explains that the net surface SW is smaller in the warm pool and the LW is smaller in the cool tongue (Table 2).

The seasonal cycle of the surface radiative fluxes (annual mean removed) is shown in Fig. 4. It focuses on the western Pacific (solid line) and eastern Pacific (dash line), respectively. In the PI simulation, the net radiative fluxes on both sides of the basin follow the semi-annual insolation forcing (Fig. 3c) and exhibits two peaks in spring and autumn (Fig. 4a). Even through the insolation forcing is uniform along the tropical Pacific, the seasonal timing of maximum and minimum heat fluxes at the surface are different in the western Pacific and eastern Pacific (Fig. 4a). Clement et al. (1999)

Early and Mid-Holocene climate in the tropical Pacific

Y. Luan et al.

Title Page

Abstract

Introduction

Conclusions

References

Tables

Figures



Back

Close

Full Screen / Esc

Printer-friendly Version

Interactive Discussion



illustrated that the background seasonal cycle in the wind divergence field is responsible for converting the zonally uniform solar forcing into a zonally asymmetric response. They showed that a uniform heating, which approximates the precessional forcing, will initially generate a uniform SST anomaly that affect the atmosphere differently in different seasons because of the background seasonal cycle in the wind divergence field. However they ignored the effect of cloud radiative forcing (CRF).

We calculated the annual mean shortwave CRF and seasonal evolution of the shortwave and longwave CRFs, using the downward shortwave and longwave fluxes at the surface in the cloudy sky minus those in the clear sky and compare it with the ISCCP data (Zhang et al., 2004) from 1984 to 1999 in Fig. 5. The annual mean shortwave CRF mainly weakens the shortwave radiation. The pattern of the cloud shortwave radiation is well simulated in the tropical Pacific. However, in the north of the equator, the signature of the CRF on the ITCZ region is too pronounced in the western tropical Pacific and underestimated in the eastern Pacific. The lack of marine stratocumulus clouds in the northeast part of the tropical Pacific is a major issue. In the south of the equator, the effect of the CRF is almost correct between 0° and 5° S but strongly underestimated along the Peru and Chile coast. The effect of clouds is maximal in the western tropical Pacific from November to March, reducing the net solar radiation at the surface. In boreal summer, the effect is smaller. In the eastern Pacific, the maximum effect of clouds on the shortwave radiation occurs in autumn. During the first half of the year, the differences in shortwave CRF between the west and the east is consistent with the different timing in the net shortwave radiation at the surface, that is characterized by a radiative cooling in the west when the east reverses to minimum cloud effect (Fig. 5). The seasonal variation of the longwave radiative forcing is small in the western tropical Pacific and enhances the net longwave radiation in the eastern tropical Pacific in autumn.

Compared to the PI simulation, increased insolation during the early and mid-Holocene causes a decrease in the net total heat flux in boreal winter and an increase in summer (Fig. 4b and d). The magnitude of the change in the net heat flux seasonal

Early and Mid-Holocene climate in the tropical Pacific

Y. Luan et al.

[Title Page](#)[Abstract](#)[Introduction](#)[Conclusions](#)[References](#)[Tables](#)[Figures](#)[⏪](#)[⏩](#)[◀](#)[▶](#)[Back](#)[Close](#)[Full Screen / Esc](#)[Printer-friendly Version](#)[Interactive Discussion](#)

cycle is larger than that of the net solar radiation, which stresses that SST, water vapor and cloud feedbacks play an important role. The maximum amplitude of the net surface heat flux is larger in the western tropical Pacific than in the eastern tropical Pacific. It results from the phase relationship between the PI cloud forcing and the insolation changes, with maximum and minimum cloud effect corresponding to decreased and increased insolation forcing at 9.5 ka or 6 ka (Figs. 4 and 5). Even though the differences with the pre-industrial values are similar for the mid and early Holocene, the magnitude is smaller for the mid-Holocene and, following the insolation forcing, minimum and maximum changes occurs in spring and late summer. The differences between the two periods reach about 10 Wm^{-2} .

4.3 Mean climate's response to orbital forcing

Figure 6 shows the simulated changes in annual mean SST, heat content and wind stress averaged from 5° S to 5° N . The annual mean SST decreases in early and mid-Holocene along the equator and is characterized by a “U” shape across the basin, with lower annual mean SST drop on both side of the basin and a larger decrease from 160° E to 120° W (Fig. 6a). Interestingly the annual mean change in ocean heat content averaged over the first 300 m has a very different structure, with increased heat content in the west from 130° E to 180° E and decreased heat content in the eastern tropical Pacific (Fig. 6b). Compared to early Holocene, the annual mean SST and heat content changes are smaller in mid-Holocene, which is consistent with the insolation forcing. The annual mean zonal SST cooling during the mid-Holocene is similar to the results of Brown et al. (2008) using the HadCM3.0 model, in which it was attributed to the reduced annual mean insolation over the tropics. Figure 6c and d show that the easterly trade winds become stronger in the western and central tropical Pacific, which is consistent with the “U” shape in SST changes and increased heat content in the western Pacific. Changes in mean wind is stronger at 9.5 ka with an increase in zonal wind twice as big as at 6 ka west of 160° W and changes in meridional wind twice as big as at 6 ka east of 160° W . As discussed in the introduction, the mean changes in

Early and Mid-Holocene climate in the tropical Pacific

Y. Luan et al.

Title Page

Abstract

Introduction

Conclusions

References

Tables

Figures



Back

Close

Full Screen / Esc

Printer-friendly Version

Interactive Discussion



Early and Mid-Holocene climate in the tropical Pacific

Y. Luan et al.

Title Page

Abstract

Introduction

Conclusions

References

Tables

Figures

◀

▶

◀

▶

Back

Close

Full Screen / Esc

Printer-friendly Version

Interactive Discussion



mid-Holocene equatorial Pacific SST and associated changes in precipitation are not strongly constrained by the available proxy records. Our results further suggest that the Niña-like mean SST response discussed in some papers is not identified from the SST, but from the changes in the mixed layer characteristics, which may explain some of the mismatches between the previous studies (Sandweiss et al., 1996; Gagan et al., 1998; Tudhope et al., 2001; Stott et al., 2004).

The differences of SST seasonal cycle (annual mean removed) between Holocene simulations and PI simulation along the equator are shown in Fig. 7. In the Early Holocene, SST is cooler in winter and warmer in summer in the tropical Pacific which is consistent with the changes in insolation. In the eastern tropical Pacific, the maximum SST changes occur in August with about one month delay compared to the maximum insolation changes (Fig. 3c). The model simulates larger SST anomalies in the eastern Pacific than in the western Pacific despite being forced by a zonally uniform insolation change, reflecting the role of dynamical atmosphere-ocean coupling in controlling SSTs in this region. SST differences propagate from the eastern tropical Pacific to the western tropical Pacific. The maximum of SST anomalies has one month lag in the western Pacific (Fig. 7a), consistent with the differences in heat fluxes discussed above. Note also that the insolation forcing reinforces the seasonal cycle of SST in the west Pacific and damps it in the east. The MH simulation exhibits similar changes (Fig. 7b). However, SST in mid-Holocene is colder in summer and warmer in winter than SST in early Holocene (Fig. 7c).

Differences between SST and heat content changes are also found in the seasonal evolution of the SST and 300 m heat content gradients across the Pacific (Fig. 8). This gradient is computed using the average over two boxes located on the western part (120° E–160° E, 5° S–5° N) and the eastern part (150° W–90° W, 5° S–5° N) of the Pacific Ocean, respectively. It is positive all year long which corresponds to the mean difference between the west where the thermocline is deep and the east Pacific where the thermocline is shallow. In the PI simulation the SST gradient is maximum during the development phase of the upwelling in boreal summer and autumn, whereas the heat

Early and Mid-Holocene climate in the tropical Pacific

Y. Luan et al.

Title Page

Abstract

Introduction

Conclusions

References

Tables

Figures



Back

Close

Full Screen / Esc

Printer-friendly Version

Interactive Discussion



content gradient is larger in boreal spring (Fig. 8). Compared to the PI simulation, the increased SST gradient in the EH simulation is slightly reduced from May to October due to the warming in the eastern Pacific and the decreased SST gradient has a strong decline in winter due to the cooling (Fig. 8a). Changes of the whole heat content above 300 m in the ocean are consistent with the SST changes. However, the weakened heat content gradient occurs about one month earlier and demises about two months earlier (Fig. 8b), indicating that subsurface temperature is warming or cooling earlier than the surface temperature. The annual mean evolution of this gradient is similar in EH and MH simulations, despite the shift in the insolation forcing. It has comparable magnitude with present day conditions for SST and is larger for heat content.

The larger changes in seasonality are found in the eastern Pacific where dynamical processes strengthen the SST response. In boreal winter (DJF), greater cooling in the eastern Pacific and warming confined to the western Pacific warm pool cause easterly wind stress anomalies in the western and central equatorial Pacific and anti-cyclone wind stress anomalies outside the tropics. Meanwhile, precipitation is reduced in the tropical Pacific. Precipitation associated with the south Pacific convergence zone (SPCZ) is intensified and shifted southward (Fig. 9). The easterly wind stress anomalies reinforce the thermocline tilt in the tropical ocean (Fig. 10). The positive subsurface temperature anomaly associated with the deepened thermocline in the western Pacific propagates along the thermocline to the central tropical Pacific in spring (MAM). However, cold SST anomalies are found at the surface throughout the basin. During boreal summer, the positive subsurface temperature anomaly reaches the east tropical Pacific and causes the thermocline depth (20°C isotherm) deepening. At the same time, increased insolation causes surface warming, and in turn leads to positive SST anomalies on the surface. In the east tropical Pacific, convergent wind stress anomalies (Fig. 9) in response to the positive SST anomalies dump the upwelling. All those processes induce the warmer SST in the eastern Pacific than in the western Pacific. Meanwhile, the negative temperature anomalies in the subsurface occur in the western tropical Pacific. The wind induced dynamical changes and propagation of the signal

at the depth of the thermocline explains that the maximum changes in temperature are found at depth and not at the surface (Fig. 10). Precipitation is increased in JJA in the eastern tropical Pacific. In boreal autumn, the cooling subsurface temperature propagates from the western tropical Pacific enhances the upwelling in eastern tropical Pacific (Fig. 11) and results in a modest weakening of equatorial thermocline depth from September.

4.4 Interannual variability characteristics

The insolation forcing together with the changes in the mean state also have an impact on the characteristics of the interannual variability. The increased boreal summer insolation enhances the Indian and Southeast Asian monsoon, as well as the inter-hemispheric SST gradient in the Pacific, during the early and mid-Holocene (Marzin and Braconnot, 2009). As the Asian monsoon interacts with ENSO in the modern climate background (Webster and Yang, 1992), changes in the strength of the monsoon may play a role in modulating ENSO amplitude in Holocene. Previous studies have identified the influence of a stronger Asian monsoon driving stronger Pacific easterly trade winds through the atmospheric Walker Circulation in boreal summer, leading to a damping of El Niño SST anomalies (Liu et al., 2000). In addition, the increased inter-hemispheric SST gradient also strengthens the easterly trade wind in the middle of the tropical Pacific and subtropical Pacific directly. Our simulations simulate a similar strengthening of the trade winds during boreal summer in the western and middle equatorial Pacific. As discussed in Braconnot et al. (2011) the magnitude of El Niño and La Niña events is damped. The larger differences were found for the EH simulation in the Niño3 box. The differences appear to be statistically significant in the east during the development phase of the events.

Braconnot et al. (2011) only present the evolution of the El Niño and La Niña composite considering the Niño3 box. Here we show in Fig. 12 the El Niño composite for SST, precipitation and wind stress anomalies in EH and MH simulations over the tropical Pacific to better highlight the patterns, and regional differences with the PI simulation.

Early and Mid-Holocene climate in the tropical Pacific

Y. Luan et al.

Title Page

Abstract

Introduction

Conclusions

References

Tables

Figures



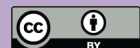
Back

Close

Full Screen / Esc

Printer-friendly Version

Interactive Discussion



**Early and
Mid-Holocene climate
in the tropical Pacific**Y. Luan et al.

[Title Page](#)[Abstract](#)[Introduction](#)[Conclusions](#)[References](#)[Tables](#)[Figures](#)[Back](#)[Close](#)[Full Screen / Esc](#)[Printer-friendly Version](#)[Interactive Discussion](#)

Figure 13 shows the difference in SST and highlights the regions where they are significant from student T-tests using the dispersion between the different events to compute the confidence interval. The characteristics of the El Niño events in Early and Mid-Holocene resemble those of the PI simulation described in Sect. 3.2. Some differences, such as the one month delay, can be depicted by eyes in the central part of the basin and at the coast (Fig. 12). In the EH simulation, the positive SST anomalies starts in June in the eastern Pacific, and is accompanied by a westerly wind stress anomalies in the western tropical Pacific and a positive precipitation anomalies in the eastern tropical Pacific (Fig. 12). Figure 13 highlights that the magnitude of the event is significantly damped in the middle of the basin in August and that this damping propagates to the east and to the west in subsequent months. In the western part SSTs are warmer than in the PI simulations. Significant differences are also found outside the equatorial band, such as in the southwestern tropical Pacific. The horse shape of these differences reflects an overall damping of the El Niño development across the basin. Along the equator, the mean state prevents the propagation of the downwelling Kelvin wave during the development phase of the event. Indeed, during that period, both the east-west temperature and heat content gradients are already relaxed compared to the pre-industrial conditions (Fig. 8). Two effects therefore counteract the developments of the anomalies, the propagation of a downwelling wave along the thermocline in the mean state and the upwelling of warmer water than in the PI simulation in the east limit the surface warming. Then at the peak of the event the propagation of the upwelling wave and the strengthening of the east-west temperature and heat content gradients in response to the mean wind further damp the intensity of the events, and contribute to delay by about one month its termination (Fig. 12). Figure 13 clearly shows that the largest differences with present day occur along the east coast and in the middle of the basin. The events also produce warm anomalies further west compared to PI simulation.

The MH simulation also produces decreased El Niño amplitude compared to PI simulation. But compared to the EH simulation, the MH SST anomalies have a smaller

magnitude during the El Niño onset (May-June) along the equator. The peak El Niño amplitude is thus larger in the eastern Pacific (Fig. 13), suggesting that El Niño was present throughout the Holocene but underwent a steady increase from the early Holocene to mid-Holocene, and then to the present day. One of the possible reasons is that insolation seasonality is larger in EH (Fig. 3c) and the EH gets more surface heat flux in summer (Fig. 4c), inducing the changes in the magnitude of the SST and heat content gradients are larger at EH. The major differences with EH simulation occurs along the coast and propagate westward. This suggests that the Chile and Peru coastal regions are the regions where the larger changes may have been recorded between the early and mid-Holocene. Substantial differences are also found in the southwest Pacific. As noted in Sect. 4.3, the changes in SST and heat content gradients are in phase for EH and MH despite the one month delay insolation between the two periods. This is certainly the reason why the timing of the El-Niño event is similar for the two periods.

Figure 14 presents similar diagnoses for La Niña years. The EH and MH simulations produce a decrease in La Niña amplitude compared to PI simulation and the differences are significant. However, La Niña amplitude has a slightly increase in the early Holocene compared to the mid-Holocene but without statistical significant. This reduction is also linked to the mean state. The intensification of the mean state during a La Niña year is associated to the westward advection of warmer than PI simulation water along the equator, resulting from the damping of the equatorial upwelling, thereby limiting the cooling effect compared to PI simulation. As for the El Niño events, significant differences are found along the coast of Chile and in the southwest Pacific.

5 The role of the obliquity

The insolation forcing considered in the MH and EH simulation results both from changes in precession and in obliquity. Precession controls the seasonal variations

CPD

8, 505–555, 2012

Early and Mid-Holocene climate in the tropical Pacific

Y. Luan et al.

Title Page

Abstract

Introduction

Conclusions

References

Tables

Figures



Back

Close

Full Screen / Esc

Printer-friendly Version

Interactive Discussion



**Early and
Mid-Holocene climate
in the tropical Pacific**

Y. Luan et al.

Title Page

Abstract

Introduction

Conclusions

References

Tables

Figures



Back

Close

Full Screen / Esc

Printer-friendly Version

Interactive Discussion



of insolation whereas obliquity controls the contrast between low and high latitudes. A reduction in obliquity increases the meridional gradient of the annual mean insolation. It also strengthens the magnitude of the seasonal cycle in both hemispheres. During the Early Holocene period, the obliquity ($\varepsilon = 24.231$) was larger than that in present day ($\varepsilon = 23.446$) (Marzin and Braconnot, 2009). Clement et al. (2004) shows the importance of precessional signals in past variations of the tropical climate using an atmospheric general circulation model coupled to a slab ocean model. However, they did not consider the interannual variability in the tropical Pacific because of the absence the full interactive ocean dynamics. In order to discuss the roles of the precession and obliquity in affecting the tropical climate respectively, we further study the impact of obliquity on the characteristics of the seasonal cycle and ENSO. We consider a 440 years long sensitivity experiment (EHOB) in which the orbital parameters are prescribed to those of pre-industrial simulation except obliquity that is set to its early Holocene value ($\varepsilon = 24.231$) as in the EH simulation. The EHOB simulation was forced with the same greenhouse gases concentration, vegetation coverage, continental ice sheets and topography as in the PI simulation. We consider the last 229 years to compute the climatological seasonal cycle.

The increase in the obliquity from 23.446 to 24.231 slightly reduces the annual mean insolation at the equator by 1.0 Wm^{-2} . However, it causes a larger increase by 5.0 Wm^{-2} in middle and high latitudes (Fig. 15). The orbital forcing also intensifies the seasonal contrast at each latitude, because of an increase of the summer hemisphere insolation and a reduction of the winter hemisphere insolation (Fig. 15a). However, in the equatorial Pacific, the seasonal cycle of the insolation is only intensified by 1.0 Wm^{-2} in the EHOB simulation. Note that the obliquity slightly enhances the seasonal cycle but does not modulate its seasonal timing. The modulation of the timing and shape of the seasonal cycle in EH and MH is induced by the precession changes (Fig. 15b).

Mantsis et al. (2011) discussed the effect of a reduction in obliquity showing that it generally increases the surface temperature at low latitudes and decreases it at high

latitudes. The direct obliquity forcing is mainly balanced by the poleward heat transport. They also showed that the changes of temperature in the subtropics and parts of the tropics are affected by the strong influence of feedbacks; in which, clouds and the lapse rate have the larger contribution. Our simulations confirm these results. The coupled system responds to the change in obliquity by a slight strengthening of the ocean and atmospheric circulation and increases the poleward transport. Liu et al. (2003) further indicates that the annual mean tropical cooling during Holocene mainly results from the annual mean insolation forcing. The comparison of the simulated annual mean changes in SST (Fig. 16) show that this holds in our study and contributes to the about 0.2°C tropical cooling simulate in both simulations. Note however that regional changes are larger at 9.5 ka due to changes in upwelling intensity induced by precession.

Annual mean tropical cooling and the changes in the meridional SST gradient have a slight impact on the location of the ITCZ. Figure 16 suggests that the annual mean tropical cooling induces a reduction in annual mean precipitation around 5°S and an increase between the equator and 5°N across Panama those are reinforced with precession. South America and the Indonesian sector are more sensitive, even though the signal is small. At the seasonal time scale (not shown), several SST pattern in SST and precipitation look quite similar in the 9.5 ka and EHOB simulation, suggesting that the seasonal march of the ITCZ in South America and In Asia is strongly linked to the meridional temperature gradients. However, our results confirm that the magnitudes of the changes are driven by precession in all regions.

The changes in the mean state are not sufficient to alter ENSO characteristics in EHOB simulation compared to EH simulation (Fig. 17). Indeed in Niño3 area, SST seasonality in the eastern Pacific is very similar to the PI simulation. The amplitude of the El Niño does not change compared to the PI simulation too. The precession is more important than obliquity in affecting the tropical Pacific SST seasonality and interannual variability. This reinforces the hypothesis changes in the seasonality of the mean background climate state is the major driver of ENSO changes during the

Early and Mid-Holocene climate in the tropical Pacific

Y. Luan et al.

Title Page

Abstract

Introduction

Conclusions

References

Tables

Figures



Back

Close

Full Screen / Esc

Printer-friendly Version

Interactive Discussion



mid-Holocene, and that in the Pacific the strengthening of the wind stress across the equator in summer and in the east Pacific in late summer has a major control on the development of ENSO.

6 Discussion and conclusions

Using a coupled ocean-atmosphere general circulation model IPSL_CM4, this study presents how the orbital forcing affects the tropical Pacific SST seasonality and inter-annual variability behavior. The simulations for the 0, 6, 9.5 ka BP climates are compared. They only account for the differences in orbital configuration. These simulations show that the amplitude of the SST seasonal variation decreases at 6 and 9.5 ka BP, compared to the 0 ka simulation. The ENSO amplitude also reduced in EH and MH simulations, which is consistent with proxy records (Rodbell et al., 1999; Moy et al., 2002), with the larger reduction in EH simulation. However, the slow variation of the insolation forcing during the Holocene has a larger impact on SST seasonality than on interannual variability even in the eastern tropical Pacific (Braconnot et al., 2011). The analysis about the role of the obliquity shows that the obliquity change has little effect on SST seasonal cycle and interannual variability in eastern tropical Pacific in our analysis. The precession of the orbital parameter is more important in effecting the tropical climate. However, the obliquity change affects the seasonal displacement of ITCZ related to strength of SST meridional gradients.

The detail analysis indicates that the annual mean SST decreases along the whole equator (Brown et al., 2008). The striking feature is that the annual mean SST is characterized by a “U” shape across the basin, which is induced by the stronger easterly trade winds in the western and middle equatorial Pacific. The annual mean changes in ocean heat content above the upper 300m show a very different structure, with increased heat content in the west from 130° E to 180° E and decreased heat content in the east tropical Pacific due to enhanced easterly winds. The amplitude of the SST seasonality decreases, with negative SST changes in winter and positive SST changes in

Early and Mid-Holocene climate in the tropical Pacific

Y. Luan et al.

Title Page

Abstract

Introduction

Conclusions

References

Tables

Figures

◀

▶

◀

▶

Back

Close

Full Screen / Esc

Printer-friendly Version

Interactive Discussion



**Early and
Mid-Holocene climate
in the tropical Pacific**Y. Luan et al.

[Title Page](#)[Abstract](#)[Introduction](#)[Conclusions](#)[References](#)[Tables](#)[Figures](#)[⏪](#)[⏩](#)[◀](#)[▶](#)[Back](#)[Close](#)[Full Screen / Esc](#)[Printer-friendly Version](#)[Interactive Discussion](#)

summer in the tropical Pacific, as a result of the changes in insolation seasonal cycle. The model simulates larger SST anomalies in the eastern Pacific than in the western Pacific despite being forced by a zonally uniform insolation change, indicating the strong influence of feedbacks. The thermodynamic and dynamic feedbacks intensify the SST anomalies caused by the insolation changes. The surface heat fluxes changes are mainly affected by the insolation forcing and the cloud radiative forcing (CRF). In the PI simulation, the CRF largely reduces the shortwave radiation in the western tropical Pacific in winter, converting the zonally uniform solar forcing into a zonally asymmetric response.

Several factors contributing to the reduction in ENSO amplitude are highlighted (Table 1). The orbital forcing enhances heat contrast between two hemispheres as well as the land and the sea, which results in strengthening the southeasterly trade winds and the south Asian monsoon flow (Marzin and Braconnot, 2009). The stronger Asian monsoon finally enhances the easterly trade winds through the atmospheric Walker Circulation in boreal summer. Both factors suppress the development of warm events. In the tropical eastern Pacific, because of the southward shift of the Intertropical Convergence Zone (ITCZ) in the region of the Panama isthmus (Braconnot et al., 2007b), the northward component of the wind stress across the equator is weakened. Xie et al. (2008) showed that the northward component of the wind stress across the equator is a key driver of the upwelling near the coast. Thus, the amplitudes of the seasonal upwelling and SST decrease as a result of weakened meridional wind across the equator in the eastern Pacific. The amplitude of ENSO may be also influenced by changes in the depth and intensity of the thermocline (Meehl et al., 2001). However, Wanner (2008) suggested that as a consequence of a changing SST gradient between the Indo-Pacific warm pool and the eastern Pacific Ocean the Walker Circulation intensified in mid-Holocene and strong El Niño events occurred more frequently. In our analysis, the reduction of ENSO amplitude is affected by the mean seasonality of the mean state. In the beginning of the El Niño development, an uplift of the equatorial Pacific thermocline in the eastern equatorial Pacific is seen in the EH and MH simulations.

Early and Mid-Holocene climate in the tropical Pacific

Y. Luan et al.

Title Page

Abstract

Introduction

Conclusions

References

Tables

Figures

⏪

⏩

◀

▶

Back

Close

Full Screen / Esc

Printer-friendly Version

Interactive Discussion



This counteracts the development of the El-Niño anomalous downwelling Kelvin wave. The thermocline tilt is controlled by the cross equatorial strengthening of the trade winds and the intensification Asian summer monsoon in the extra-tropics. Meanwhile both the SST and heat content east-west gradients are relaxed compared to PI simulation and further damp the development of the events. That is also the reason why the timing of the El Niño event is similar for the two periods, even though there are differences in timing in insolation between EH and MH.

These results also show that SST anomalies have a complex structure that reflects both dynamical and thermodynamical forcings. Temperature changes are large at the thermocline depth and better reflect the changes in the wind stress forcing. Following the discussion of DiNezio et al. (2011) for the last glacial maximum, it strongly suggests that subsurface proxy records would provide a better constraint than SST proxies on the mean ocean state. Also multi-proxy integrations considering both changes in the mean state and in variability would be of great use to assess the realism of climate model and to better understand the link between seasonality and interannual variability, thus helping to improve climate predictability.

Acknowledgements. The NEC SX8 computing time requested to run the simulations has been provided by CEA (France). This study contributes to the French ANR Project ELPASO (no. 2010 BLANC 608 01), the European project Past4Future and is jointly supported by the “Strategic Priority Research Program – Climate Change: Carbon Budget and Related Issues” of the Chinese Academy of Sciences (No. XDA01020304) and China NSFC grant (No. 40975065). Yihua Luan received a PhD grant from the French Embassy in Beijing.



The publication of this article is financed by CNRS-INSU.

References

- AchutaRao, K. and Sperber, K. R.: ENSO simulation in coupled ocean-atmosphere models: are the current models better?, *Clim. Dynam.*, 27, 1–15, 2006.
- Annamalai, H., Hamilton, K., and Sperber, K. R.: The South Asian Summer Monsoon and Its Relationship with ENSO in the IPCC AR4 Simulations, *J. Climate*, 20, 1071–1092, 2007.
- Berger, A. L.: Long-term variations of daily insolation and quaternary climatic changes, *J. Atmos. Sci.*, 35, 2362–2367, 1978.
- Braconnot, P., Hourdin, F., Bony, S., Dufresne, J. L., Grandpeix, J. Y., and Marti, O.: Impact of different convective cloud schemes on the simulation of the tropical seasonal cycle in a coupled ocean-atmosphere model, *Clim. Dynam.*, 29, 501–520, 2007a.
- Braconnot, P., Otto-Bliesner, B., Harrison, S., Jousseaume, S., Peterchmitt, J.-Y., Abe-Ouchi, A., Crucifix, M., Driesschaert, E., Fichet, Th., Hewitt, C. D., Kageyama, M., Kitoh, A., Laîné, A., Loutre, M.-F., Marti, O., Merkel, U., Ramstein, G., Valdes, P., Weber, S. L., Yu, Y., and Zhao, Y.: Results of PMIP2 coupled simulations of the Mid-Holocene and Last Glacial Maximum – Part 1: experiments and large-scale features, *Clim. Past*, 3, 261–277, doi:10.5194/cp-3-261-2007, 2007b.
- Braconnot, P., Luan, Y., Brewer, S., and Zheng, W.: Impact of Earth's orbit and freshwater fluxes on Holocene climate mean seasonal cycle and ENSO characteristics, *Clim. Dynam.*, doi:10.1007/s00382-011-1029-x, in press, 2011.
- Brown, J., Collins, M., and Tudhope, A.: Coupled model simulations of mid-Holocene ENSO and comparisons with coral oxygen isotope records, *Adv. Geosci.*, 6, 29–33, doi:10.5194/adgeo-6-29-2006, 2006.
- Brown, J., Collins, M., Tudhope, A. W., and Toniazzo, T.: Modelling mid-Holocene tropical climate and ENSO variability: towards constraining predictions of future change with palaeodata, *Clim. Dynam.*, 30, 19–36, 2008a.
- Brown, J., Tudhope, A. W., Collins, M., and McGregor, H. V.: Mid-Holocene ENSO: Issues in quantitative model-proxy data comparisons, *Paleoceanography*, 23, PA3202, doi:10.1029/2007PA001512, 2008b.
- Bush, A.: Assessing the impact of Mid-Holocene insolation on the atmosphere-ocean system, *Geophys. Res. Lett.*, 26, 99–102, 1999.
- Chiang, J. C. H., Fang, Y., and Chang, P.: Pacific climate change and ENSO activity in the mid-Holocene, *J. Climate*, 22, 923–939, 2009.

Early and Mid-Holocene climate in the tropical Pacific

Y. Luan et al.

Title Page

Abstract

Introduction

Conclusions

References

Tables

Figures

◀

▶

◀

▶

Back

Close

Full Screen / Esc

Printer-friendly Version

Interactive Discussion



**Early and
Mid-Holocene climate
in the tropical Pacific**Y. Luan et al.

Title Page

Abstract

Introduction

Conclusions

References

Tables

Figures

◀

▶

◀

▶

Back

Close

Full Screen / Esc

Printer-friendly Version

Interactive Discussion



- Clement, A. C., Seager, R., Cane, M. A., and Zebiak, S. E.: An ocean dynamical thermostat, *J. Climate*, 9, 2190–2196, 1996.
- Clement, A. C., Seager, R., and Cane, M. A.: Orbital controls on ENSO and tropical climate, *Paleoceanography*, 14, 441–456, 1999.
- 5 Clement, A. C., Seager, R., and Cane, M. A.: Suppression of El Niño during the mid-Holocene by changes in the Earth's orbit, *Paleoceanography*, 15, 731–737, 2000.
- Clement, A. C., Cane, M. A., and Seager, R.: An orbitally driven tropical source for abrupt climate change, *J. Climate*, 14, 2369–2375, 2001.
- Clement, A. C., Hall, A., and Broccoli, A. J.: The importance of precessional signals in the
10 tropical climate, *Clim. Dynam.*, 22, 327–341, 2004.
- Collins, M.: El Niño- or La Niña-like climate change, *Clim. Dynam.*, 24, 89–104, 2005.
- Collins, M., Tett, S. F. B., and Cooper, C.: The internal climate variability of HadCM3, a version of the Hadley Centre coupled model without flux adjustments, *Clim. Dynam.*, 17, 61–81, 2001.
- 15 DiNezio, P. N., Clement, A., Vecchi, G. A., Soden, B., Broccoli, A. J., Otto-Bliesner, B. L., and Braconnot, P.: The response of the Walker circulation to Last Glacial Maximum forcing: Implications for detection in proxies, *Paleoceanography*, 26, PA3217, doi:10.1029/2010PA002083, 2011.
- Fichefet, T. and Maqueda, M. A. M.: Sensitivity of a global sea ice model to the treatment of ice thermodynamics and dynamics, *J. Geophys. Res.*, 102, 12609–12646, 1997.
- 20 Gagan, M. K., Ayliffe, L. K., Hopley, D., Cali, J. A., Mortimer, G. E., Chappell, J., McCulloch, M. T., and Head, M. J.: Temperature and surface-ocean water balance of the mid-Holocene tropical western Pacific, *Science*, 29, 1014–1018, 1998.
- Gordon, C. T. and Stern, W.: A description of the GFDL global Spectral model, *Mon. Weather Rev.*, 110, 625–644, 1982.
- 25 Guilyardi, E.: El Niño-mean state-seasonal cycle interactions in a multi-model ensemble, *Clim. Dynam.*, 26, 329–348, 2006
- Guilyardi, E., Wittenberg, A., Fedorov, A., Collins, M., Wang, C., Capotondi, A., Oldenborgh, G. J., and Stockdale, T.: Understanding El Niño in Ocean-Atmosphere general circulation models: Progress and challenges, *B. Am. Meteorol. Soc.*, 90, 325–340,,
30 doi:10.1175/2008BAMS2387.1, 2009.
- Hewitt, C. D. and Mitchell, J. F. B.: A fully coupled GCM simulation of the climate of the mid-Holocene, *Geophys. Res. Lett.*, 25, 361–364, 1998.

Early and Mid-Holocene climate in the tropical Pacific

Y. Luan et al.

Title Page

Abstract

Introduction

Conclusions

References

Tables

Figures

◀

▶

◀

▶

Back

Close

Full Screen / Esc

Printer-friendly Version

Interactive Discussion



- Hourdin, F., Musat, I., Bony, S., Braconnot, P., Codron, F., Dufresne, J. L., Fairhead, L., Filiberti, M. A., Friedlingstein, P., Grandpeix, J. Y., Krinner, G., Levan, P., Li, Z. X., and Lott, F.: The LMDZ4 general circulation model: climate performance and sensitivity to parametrized physics with emphasis on tropical convection, *Clim. Dynam.*, 27, 787–813, 2006.
- 5 IPCC 2007: Climate Change 2007, The Physical Science Basis – Summary for Policymakers, 21 pp., 2007.
- Jacob, R.: Low frequency variability in a simulated atmosphere ocean system, Ph.D thesis, University of Wisconsin-Madison, 1997.
- Joussaume, S. and Braconnot, P.: Sensitivity of paleoclimate simulation results to season definitions, *J. Geophys. Res.*, 102, 1943–1956, 1997.
- 10 Kao, H.-Y. and Yu, J.-Y.: Contrasting eastern-Pacific and central-Pacific types of ENSO, *J. Climate*, 22, 615–632, 2009.
- Kiehl, J. T., Hack, J. J., Bonan, G. B., Boville, B. A., Williamson, D. L., and Rasch, P. J.: The National Center for Atmospheric Research Community Climate Model: CCM3, *J. Climate*, 11, 1131–1149, 1998.
- 15 Koutavas, A., Lynch-Stieglitz, J., Marchitto, T. M., and Sachs, J. P.: El Niño-like pattern in Ice Age tropical Pacific sea surface temperature, *Science*, 297, 226–230, 2002.
- Krinner, G., Viovy, N., de Noblet-Ducoudre, N., Ogee, J., Polcher, J., Friedlingstein, P., Ciais, P., Sitch, S., and Prentice, I. C.: A dynamic global vegetation model for studies of the coupled atmosphere-biosphere system, *Global Biogeochem. Cy.*, 19, GB1015, doi:10.1029/2003GB002199, 2005.
- 20 Kug, J.-S., Jin, F.-F., and An, S.: Two types of El Niño events: Cold tongue El Niño and warm pool El Niño, *J. Climate*, 22, 1499–1515, 2009.
- Latif, M., Kleeman, R., and Eckert, C.: Greenhouse warming, decadal variability, or El Niño? An attempt to understand the anomalous 1990s, *J. Climate*, 10, 2221–2239, 1997.
- 25 Latif, M., Sperber, K., Arblaster, J., Braconnot, P., Chen, D., Colman, A., Cubasch, U., Cooper, C., Delecluse, P., Dewitt, D., Fairhead, L., Flato, G., Hogan, T., Ji, M., Kimoto, M., Kitoh, A., Knutson, T., Le Treut, H., Li, T., Manabe, S., Marti, O., Mechoso, C., Meehl, G., Power, S., Roeckner, E., Sirven, J., Terray, L., Vintzileos, A., Bob, R., Wang, B., Washington, W., Yoshikawa, I., Yu, J., and Zebiak, S.: ENSIP: The El Niño simulation intercomparison project, *Clim. Dynam.*, 18, 255–276, 2001.
- 30 Lau, N. C. and Nath, M. J.: Impact of ENSO on the Variability of the Asian-Australian Monsoons as Simulated in GCM Experiments, *J. Climate*, 13, 4287–4309, 2000.

**Early and
Mid-Holocene climate
in the tropical Pacific**Y. Luan et al.

[Title Page](#)[Abstract](#)[Introduction](#)[Conclusions](#)[References](#)[Tables](#)[Figures](#)[◀](#)[▶](#)[◀](#)[▶](#)[Back](#)[Close](#)[Full Screen / Esc](#)[Printer-friendly Version](#)[Interactive Discussion](#)

- Lea, D. W., Pak, D. K., Belanger, C. L., Spero, H. J., Hall, M. A., and Shackleton, N. J.: Paleoclimate history of Galapagos surface waters over the last 135,000 yr, *Quaternary Sci. Rev.*, 25, 1152–1167, 2006.
- 5 Leloup, J., Lengaigne, M., and Boulanger, J. P.: Twentieth century ENSO characteristics in the IPCC database, *Clim. Dynam.*, 30, 277–291, 2008.
- Levitus, S.: Climatological atlas of the world ocean, *Eos Trans. AGU*, 64, 962, doi:10.1029/EO064i049p00962-02, 1983.
- Liu, Z., Jacobs, R., Kutzbach, J., Harrison, S., and Anderson, J.: Monsoon impact on El Niño variability in the early Holocene, *PAGES Newsletter*, 7, 16–17, 1999.
- 10 Liu, Z., Kutzbach, J., and Wu, L.: Modeling climate shift of El Niño variability in the Holocene, *Geophys. Res. Lett.*, 27, 2265–2268, 2000.
- Liu, Z., Otto-Bliesner, B., Kutzbach, J., Li, L., and Shields, C.: Coupled model simulation of the evolution of global monsoons in the Holocene, *J. Climate*, 16, 2472–2490, 2003.
- Madec, G., Delecluse, P., Imbard, M., and Levy, C.: OPA version 8.1 ocean general circulation model reference manual, *LODYC/IPSL*, Paris, France, 11, 1998.
- 15 Mantsis, D. F., Clement, A. C., Broccoli, A. J., and Erb, M. P.: Climate feedbacks in response to changes in obliquity, *J. Climate*, 24, 2830–2845, 2011.
- Marti, O., Braconnot, P., Dufresne, J.-L., Bellier, J., Benshila, R., Bony, S., Brockmann, P., Cadule, P., Caubel, A., Codron, F., de Noblet, N., Denvil, S., Fairhead, L., Fichefet, T., Foujols, M.-A., Friedlingstein, P., Goosse, H., Grandpeix, J.-Y., Guilyardi, E., Hourdin, F., Idelkadi, A., Kageyama, M., Krinner, G., Levy, C., Madec, G., Mignot, J., Musat, I., Swingedouw, D., and Talandier, C.: Key features of the IPSL ocean atmosphere model and its sensitivity to atmospheric resolution, *Clim. Dynam.*, 34, 1–26, 2010.
- 20 Marzin, C. and Braconnot, P.: Variations of Indian and African monsoons induced by insolation changes at 6 and 9.5 kyr BP, *Clim. Dynam.*, 33, 215–231, 2009.
- McGlone, M. S., Kershaw, A. P., and Markgraf, V.: El Niño/ Southern Oscillation climatic variability in Australasian and South American paleoenvironmental records, In *El Niño – historical and paleoclimatic aspects of the Southern Oscillation*, edited by: Diaz, H. F. and Markgraf, V., Cambridge Univ. Press, New York, 435–462, 1992.
- 30 McGregor, H. V. and Gagan, M. K.: Western Pacific coral $\delta^{18}\text{O}$ records of anomalous Holocene variability in the El Niño-Southern Oscillation, *Geophys. Res. Lett.*, 31, L11204, doi:10.1029/2004GL019972, 2004.

Early and Mid-Holocene climate in the tropical Pacific

Y. Luan et al.

Title Page

Abstract

Introduction

Conclusions

References

Tables

Figures

◀

▶

◀

▶

Back

Close

Full Screen / Esc

Printer-friendly Version

Interactive Discussion



- Meehl, G. A., Gent, P. R., Arblaster, J. M., Otto-Bliesner, B. L., Brady, E. C., and Craig, A.: Factors that affect the amplitude of El Niño in global coupled climate models, *Clim. Dynam.*, 17, 515–526, 2001.
- Meehl, G. A., Stocker, T. F., Collins, W. D., Friedlingstein, P., Gaye, A. T., Gregory, J. M., Kitoh, A., Knutti, R., Murphy, J. M., Noda, A., Raper, S. C. B., Watterson, I. G., Weaver, A. J., and Zhao, Z. C.: Global climate projections, *Climate Change 2007: The Physical Science Basis. Contribution of Working Group I to the Fourth Assessment Report of the Intergovernmental Panel on Climate Change*, edited by: Solomon, S., Qin, D., Manning, M., Chen, Z., Marquis, M., Averyt, K. B., Tignor, M., and Miller, H. L., Cambridge University Press, Cambridge, UK and New York, NY, USA, 2007.
- Merryfield, W. J.: Changes to ENSO under CO₂ doubling in the IPCC AR4 coupled climate models, *J. Climate*, 19, 4009–4027, 2006.
- Moy, C. M., Seltzer, G. O., Rodbell, D. T., and Anderson, D. M.: Variability of El Niño/Southern Oscillation activity at millennial time-scales during the Holocene epoch, *Nature*, 420, 162–165, 2002.
- Otto-Bliesner, B. L. and Brady, E. C.: Tropical Pacific variability in the NCAR Climate System Model, *J. Climate*, 14, 3587–3607, 2001.
- Otto-Bliesner, B. L., Brady, E. C., Shin, S.-I., Liu, Z., and Shields, C.: Modeling El Niño and its tropical teleconnections during the last glacial-interglacial cycle, *Geophys. Res. Lett.*, 30, 2198–2201, 2003.
- Philander, S. G.: *El Niño, La Niña, and the Southern Oscillation*, Academic Press, San Diego, ix + 293pp., 1990.
- Rayner, N. A., Parker, D. E., Horton, E. B., Folland, C. K., Alexander, L. V., Rowell, D. P., Kent, E. C., and Kaplan, A.: Global analyses of sea surface temperature, sea ice, and night marine air temperature since the late nineteenth century, *J. Geophys. Res.*, 108, 4407, doi:10.1029/2002JD002670, 2003.
- Reichler, T. and Kim, J.: How well do coupled models simulate today's climate?, *B. Am. Meteorol. Soc.*, 89, 303–311, 2008.
- Rodbell, D. T., Seltzer, G. O., Anderson, D. M., Abbott, M. B., Enfield, D. B., and Newman, J. H.: An ~15,000-year Record of El Niño–Driven Alluviation in Southwestern Ecuador, *Science*, 283, 516–520, 1999.

**Early and
Mid-Holocene climate
in the tropical Pacific**Y. Luan et al.

[Title Page](#)[Abstract](#)[Introduction](#)[Conclusions](#)[References](#)[Tables](#)[Figures](#)[◀](#)[▶](#)[◀](#)[▶](#)[Back](#)[Close](#)[Full Screen / Esc](#)[Printer-friendly Version](#)[Interactive Discussion](#)

Ropelewski, C. F. and Halpert, M. S.: North American precipitation and temperature patterns associated with the El Niño/Southern Oscillation (ENSO), *Mon. Weather Rev.*, 114, 2352–2362, 1986.

Sandweiss, D. H., Richardson, J. B., Reitz, E. J., Rollins, H. B., and Maasch, K. A.: Geographical evidence from Peru for a 5000 year B.P. onset of El Niño, *Science*, 273, 1531–1533, 1996.

Sodn, B. J. and Held, I. M.: An assessment of climate feedbacks in coupled ocean-atmosphere models, *J. Climate*, 19, 3354–3360, 2006.

Solomon, S., Qin, D., Manning, M., Chen, Z., Marquis, M., Averyt, K. B., Tignor, M., and Miller, H. L.: IPCC 2007: Climate Change 2007, The physical basis. Contribution of Working Group I to the Fourth Assessment Report of the Intergovernmental Panel on Climate change, Cambridge University Press, Cambridge, 2007.

Stott, L., Cannariato, K., Thunell, R., Haug, G. H., Koutavas, A., and Lund, S.: Decline of surface temperature and salinity in the western tropical Pacific Ocean in the Holocene epoch, *Nature*, 431, 56–59, 2004.

Terray, L., Sevault, E., Guilyardi, E., and Thual, O.: The OASIS coupler user guide version 2.0, Cerfacs technical report TR/CMGC/95-46, 123 pp., 1995.

Timmermann, A., Lorenz, S. J., An, S.-I., Clement, A., and Xie, S.-P.: The Effect of Orbital Forcing on the Mean Climate and Variability of the Tropical Pacific, *J. Climate*, 20, 4147–4259, 2007.

Tudhope, A. W., Chilcott, C. P., McCulloch, M. T., Cook, E. R., Chappell, J., Ellam, R. M., Lea, D. W., Lough, J. M., and Shimmield, G. B.: Variability in the El Niño-Southern Oscillation through a glacial-interglacial cycle, *Science*, 291, 1511–1517, 2001.

van Oldenborgh, G. J., Philip, S. Y., and Collins, M.: El Niño in a changing climate: a multi-model study, *Ocean Sci.*, 1, 81–95, doi:10.5194/os-1-81-2005, 2005.

Wang, B.: The vertical structure and development of the ENSO anomaly mode during 1979–1989, *J. Atmos. Sci.*, 49, 698–712, 1992.

Wang, B., Wu, R., and Fu, X.: Pacific-East Asian Teleconnection: How Does ENSO Affect East Asian Climate?, *J. Climate*, 13, 1517–1536, 2000.

Wang, C. and Picaut, J.: Understanding ENSO physics – A review. *Earth's Climate: The Ocean-Atmosphere Interaction*, *Geophys. Monogr.*, 147, 21–69, 2004.

Early and Mid-Holocene climate in the tropical Pacific

Y. Luan et al.

Title Page

Abstract

Introduction

Conclusions

References

Tables

Figures

◀

▶

◀

▶

Back

Close

Full Screen / Esc

Printer-friendly Version

Interactive Discussion



- Wanner, H., Beer, J., Butikofer, J., Crowley, T. J., Cubasch, U., Fluckiger, J., Goosse, H., Grosjean, M., Joos, F., Kaplan, J. O., Kuttel, M., Muller, S. A., Prentice, I. C., Solomina, O., Stocker, T. F., Tarasov, P., Wagner, M., and Widmann, M.: Mid- to Late Holocene climate change: an overview, *Quaternary Sci. Rev.*, 27, 1791–1828, 2008.
- 5 Webster, P. J. and Yang, S.: Monsoon and ENSO: Selectively interactive systems, *Q. J. Roy. Meteorol. Soc.*, 118, 877–926, 1992.
- Wen, X. Y., Wang, S. W., and Zhu, J. H.: An overview of the paleo-ENSO, *Chinese J. Geophys.*, 50, 387–396, 2007.
- 10 Wright, H., Kutzbach, J., Webb III, T., Ruddiman, W., Street-Perrot, F., Bartlein, P.: *Global climates since the last glacial maximum*, University of Minnesota Press, 1993.
- Yeh, S.-W., Kug, J.-S., Dewitte, B., Kwon, M.-H., Kirtman, B. P., and Jin, F.-F.: El Niño in a changing climate, *Nature*, 461, 511–674, 2009.
- Zebiak, S. E. and Cane, M. A.: A model El Nino-Southern Oscillation, *Mon. Weather Rev.*, 115, 2262–2278, 1987.
- 15 Zhang, Y., Rossow, W. B., Lacis, A. A., Oinas, V., and Mishchenko M. I.: Calculation of radiative fluxes from the surface to top of atmosphere based on ISCCP and other global data sets: Refinements of the radiative transfer model and the input data, *J. Geophys. Res.*, 109, D19105, doi:10.1029/2003JD004457, 2004.
- 20 Zheng, W., Braconnot, P., Guilyardi, E., Merkel, U., and Yu, Y.: ENSO at 6 ka and 21 ka from ocean-atmosphere coupled model simulations, *Clim. Dynam.*, 30, 745–762, 2008.

Table 1. Paleo-ENSO simulations.

authors	model	periods	conclusions
Clement et al. (1999, 2000, 2001)	Zebiak-Cane model (Zebiak and Cane, 1987)	Mid-Holocene	The changes of tropical Pacific climate over the mid- to late Holocene is largely induced by orbitally driven changes in the seasonal cycle of solar radiation in the tropics
Bush (1999)	GFDL AGCM (Gordon and Stern 1982)	6 ka	A coupled AOGCM produce enhanced Pacific upwelling, a more pronounced cold tongue, and an even stronger monsoon. The climate of the equatorial Pacific was more similar to the La Niña phase of the modern Southern Oscillation
Liu et al. (2000)	FOAM (Jacob R., 1997)	Early and mid-Holocene (11 ka and 6 ka)	ENSO intensity reduced by both an intensified Asian summer monsoon and a South Hemisphere warm water subduction caused by insolation changes
Otto-Bliesner et al. (2003)	CSM (Otto-Bliesner and Brady, 2001)	LGM (21 ka) and Holocene (11 ka)	Model predicted weaker El Niños/La Niñas compared to present for the Holocene and stronger El Niños/La Niñas for the LGM.
Brown et al. (2008a,b)	HadCM3 (Collins et al., 2001)	6 ka	The model simulates a smaller reduction in ENSO amplitude of around 10 %, and it also simulates a slight shift to longer period variability and a weakening of ENSO phase-locking to the seasonal cycle in the
mid-Holocene.			
Zheng et al. (2008)	PMIP2 models	LGM (21 ka) and mid-Holocene (6 ka)	Results from an ensemble of mid-Holocene simulations run with different climate models as part of PMIP2 show a reduced simulated El Niño amplitudes at 6 ka than at present

Early and Mid-Holocene climate in the tropical Pacific

Y. Luan et al.

Title Page

Abstract

Introduction

Conclusions

References

Tables

Figures

◀

▶

◀

▶

Back

Close

Full Screen / Esc

Printer-friendly Version

Interactive Discussion



Early and Mid-Holocene climate in the tropical Pacific

Y. Luan et al.

Table 1. Continued.

authors	model	periods	conclusions
Chiang et al. (2009)	CCM3 (Kiehl et al., 1998)	Mid-Holocene	The mid-Holocene ENSO reduction was in response to Pacific-wide climate changes to mid-Holocene orbital conditions
Braconnot et al. (2011)	IPSL_CM4 (Marti et al., 2010)	0 ka, 6 ka and 9.5 ka	The insolation forcing affects both the tropical Pacific SST seasonal cycle and ENSO characteristics and the resulting changes have a larger magnitude than that the changes induced by a fresh water flux release in the north Atlantic. Holocene SST changes are dominated by changes in seasonality in most of the tropical Pacific.

Title Page

Abstract

Introduction

Conclusions

References

Tables

Figures

◀

▶

◀

▶

Back

Close

Full Screen / Esc

Printer-friendly Version

Interactive Discussion



Early and Mid-Holocene climate in the tropical Pacific

Y. Luan et al.

Table 2. Annual mean radiative flux in the western Pacific (WP: 140° E–180° E, 5° S–5° E) and the Niño3 box (150° W–90° W, 5° S–5° E) (Wm^{-2} , positive downward).

		TOTAL	SW	LW	HS	LE
0 ka	WP	32.71	232.90	-73.25	-14.85	-112.37
	Niño3	92.33	249.72	-59.43	-10.15	-87.80
6 ka	WP	36.02	237.82	-74.68	-15.02	-112.40
	Niño3	91.53	250.70	-59.98	-10.40	-88.79
9.5 ka	WP	37.90	240.72	-75.40	-15.09	-112.63
	Niño3	91.15	250.15	-60.15	-10.46	-88.39

Title Page

Abstract

Introduction

Conclusions

References

Tables

Figures

◀

▶

◀

▶

Back

Close

Full Screen / Esc

Printer-friendly Version

Interactive Discussion



Early and
Mid-Holocene climate
in the tropical Pacific

Y. Luan et al.

Title Page

Abstract

Introduction

Conclusions

References

Tables

Figures



Back

Close

Full Screen / Esc

Printer-friendly Version

Interactive Discussion

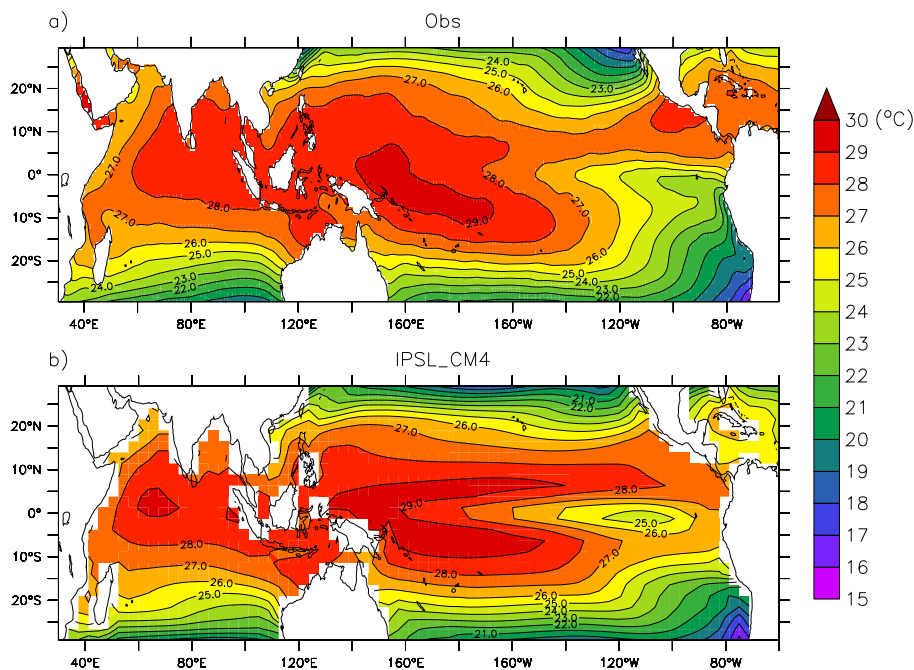


Fig. 1. Annual mean SST ($^{\circ}\text{C}$) distributions in the tropical Pacific and Indian Ocean: **(a)** observed climatology HadISST data from 1870 to 2003 and **(b)** IPSL_CM4 PI simulation.

Early and Mid-Holocene climate in the tropical Pacific

Y. Luan et al.

Title Page

Abstract

Introduction

Conclusions

References

Tables

Figures

◀

▶

◀

▶

Back

Close

Full Screen / Esc

Printer-friendly Version

Interactive Discussion

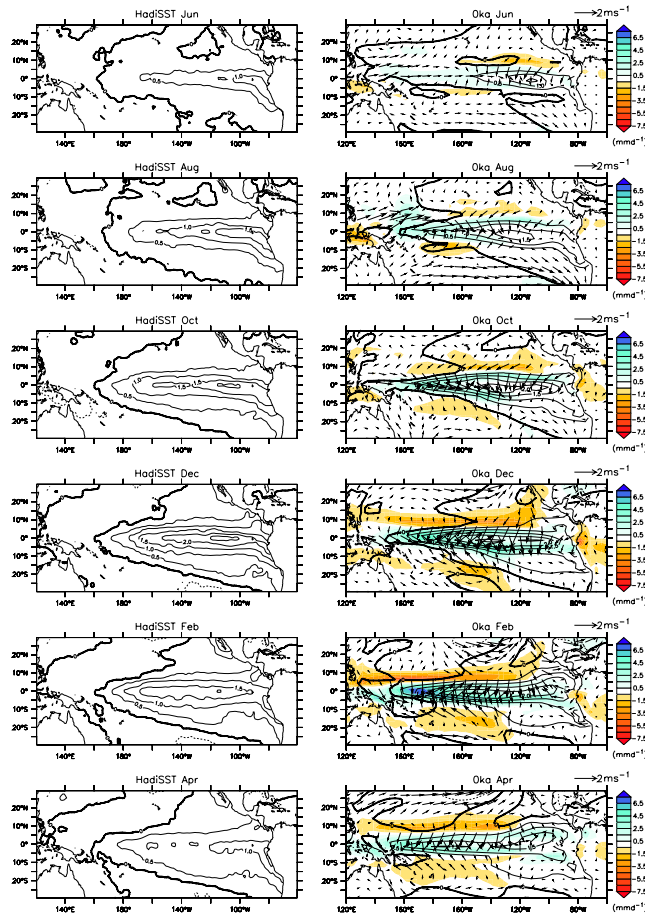


Fig. 2. The evolution of SST (line, °C), precipitation (color, mm d^{-1}) and wind stress anomalies (arrow, m s^{-1}) during a composite El Niño year in the PI simulation (see details of the composite analysis in the text), compared to the similar evolution of SST (line, °C) in HadISST data (Rayner et al., 2003).

Early and Mid-Holocene climate in the tropical Pacific

Y. Luan et al.

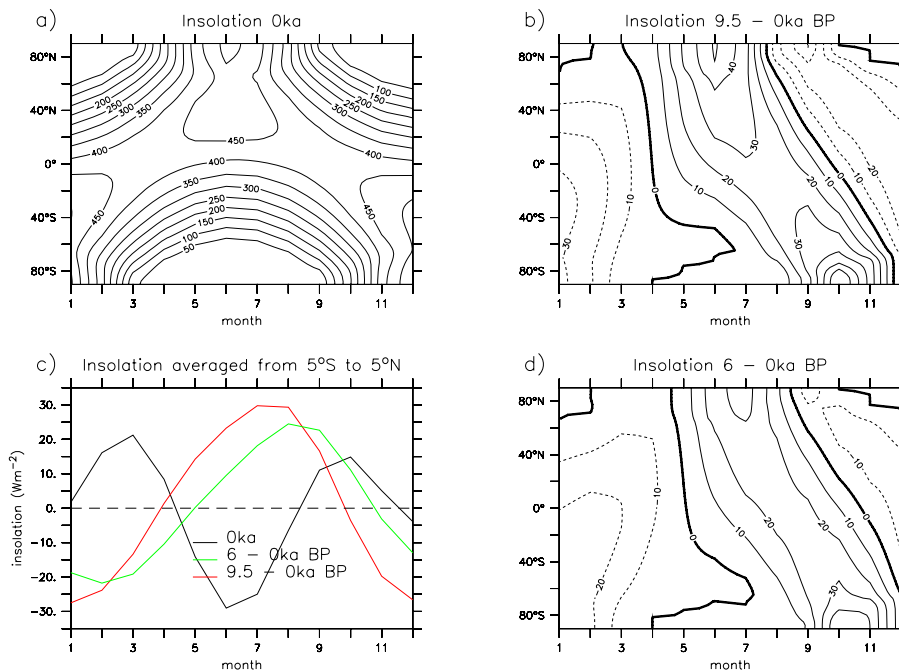


Fig. 3. Incoming solar radiation (Wm^{-2}) at the top of the atmosphere plotted as a function of months and latitude for **(a)** 0 ka BP, **(b)** 9.5–0 ka BP, **(d)** 6–0 ka BP; **(c)** insolation averaged from 5° S to 5° N (annual mean removed) and plotted as a function of months for 0 ka (black line), 6–0 ka BP (green line) and 9.5–0 ka BP (red line).

Title Page

Abstract

Introduction

Conclusions

References

Tables

Figures

◀

▶

◀

▶

Back

Close

Full Screen / Esc

Printer-friendly Version

Interactive Discussion

Early and Mid-Holocene climate in the tropical Pacific

Y. Luan et al.

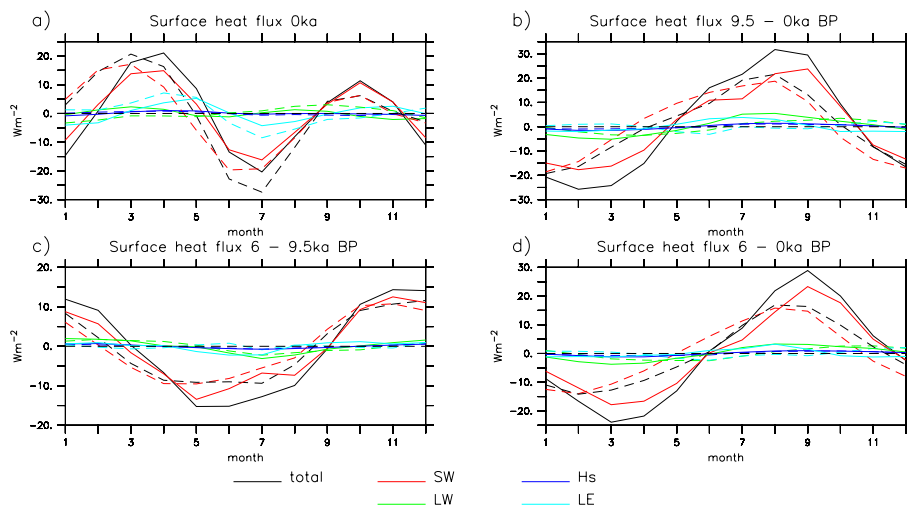


Fig. 4. Changes in the seasonal evolution of surface heat flux (Wm^{-2}) (annual mean removed) for the western Pacific (140°E – 180°E , 5°S – 5°N) (solid line) and the eastern Pacific (90°W – 150°W , 5°S – 5°N) (dash line). Surface heat fluxes include the net solar radiation (SW, positive downward), the net longwave radiation (LW, positive downward), the latent heat flux (LE, positive downward), the sensible heat flux (Hs, positive downward), and the net heat flux (surface budget = $\text{SW} + \text{LW} + \text{LE} + \text{Hs}$, positive downward).

Title Page

Abstract

Introduction

Conclusions

References

Tables

Figures

⏪

⏩

◀

▶

Back

Close

Full Screen / Esc

Printer-friendly Version

Interactive Discussion



Early and Mid-Holocene climate in the tropical Pacific

Y. Luan et al.

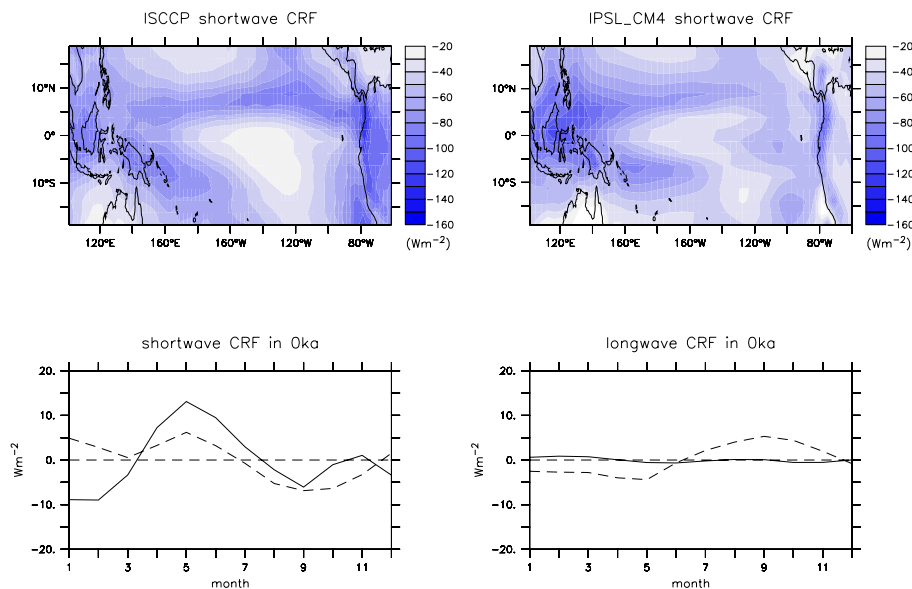


Fig. 5. Annual mean shortwave cloud radiative forcing (CRF) (Wm^{-2}) for the observed ISCCP data (Zhang et al., 2004) from 1984 to 1999 and IPSL_CM4 PI simulation (upper panels); seasonal cycle of the shortwave and longwave CRF (Wm^{-2} , annual mean removed) at the surface in PI simulation for the western Pacific (140°E – 180°E , 5°S – 5°N) (solid line) and the eastern Pacific (90°W – 150°W , 5°S – 5°N) (dash line) (lower panels).

[Title Page](#)
[Abstract](#)
[Introduction](#)
[Conclusions](#)
[References](#)
[Tables](#)
[Figures](#)
[Back](#)
[Close](#)
[Full Screen / Esc](#)
[Printer-friendly Version](#)
[Interactive Discussion](#)

Early and Mid-Holocene climate in the tropical Pacific

Y. Luan et al.

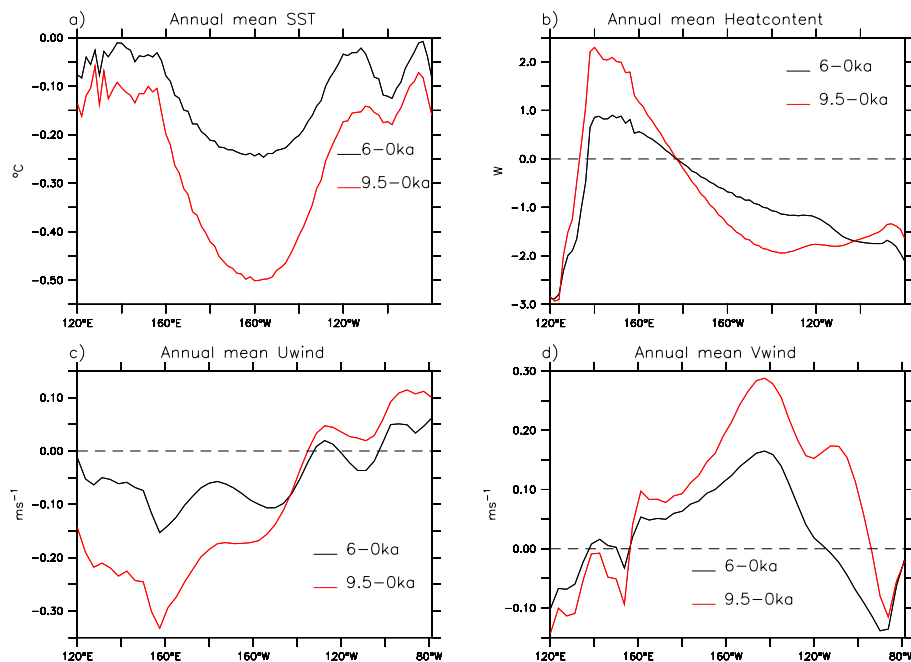


Fig. 6. Changes in annual mean **(a)** SST (°C), **(b)** heat content (W), **(c)** surface zonal wind ($m s^{-1}$) and **(d)** surface meridional wind ($m s^{-1}$) along the equator (averaged between 5° S and 5° N).

Title Page

Abstract

Introduction

Conclusions

References

Tables

Figures

◀

▶

◀

▶

Back

Close

Full Screen / Esc

Printer-friendly Version

Interactive Discussion



Early and Mid-Holocene climate in the tropical Pacific

Y. Luan et al.

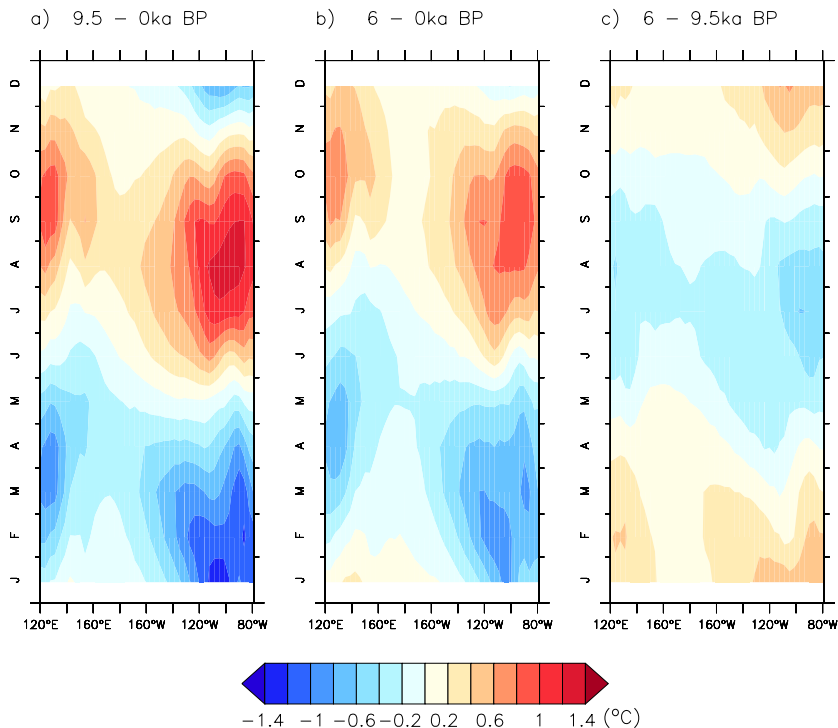


Fig. 7. Differences of the SST ($^{\circ}\text{C}$) seasonal cycle (annual mean removed) between Holocene simulations and PI simulation averaged from 5°S to 5°N in the tropical Pacific for **(a)** 9.5–0 ka, **(b)** 6–0 ka, **(c)** 6–9.5 ka.

Title Page

Abstract

Introduction

Conclusions

References

Tables

Figures

◀

▶

◀

▶

Back

Close

Full Screen / Esc

Printer-friendly Version

Interactive Discussion



Early and Mid-Holocene climate in the tropical Pacific

Y. Luan et al.

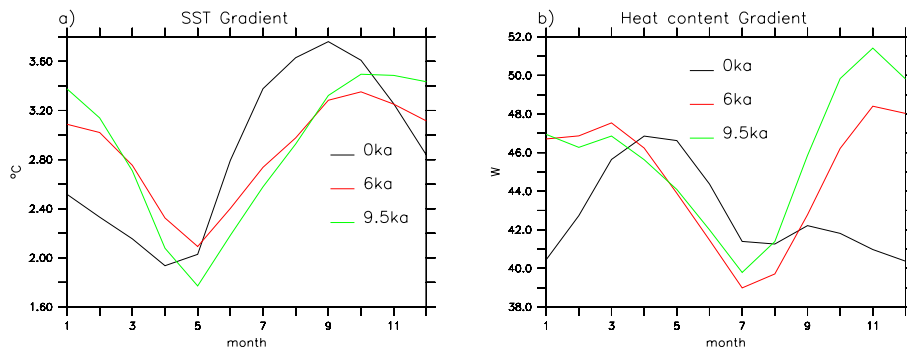


Fig. 8. The mean annual evolution of **(a)** the SST ($^{\circ}\text{C}$) and **(b)** 300 m heat content (W) gradients, computed as the different values of the averaged western Pacific (140°E – 180°E , 5°S – 5°N) and the averaged eastern Pacific (150°W – 90°W , 5°S – 5°N) for the different simulations.

Title Page

Abstract

Introduction

Conclusions

References

Tables

Figures

◀

▶

◀

▶

Back

Close

Full Screen / Esc

Printer-friendly Version

Interactive Discussion



Early and Mid-Holocene climate in the tropical Pacific

Y. Luan et al.

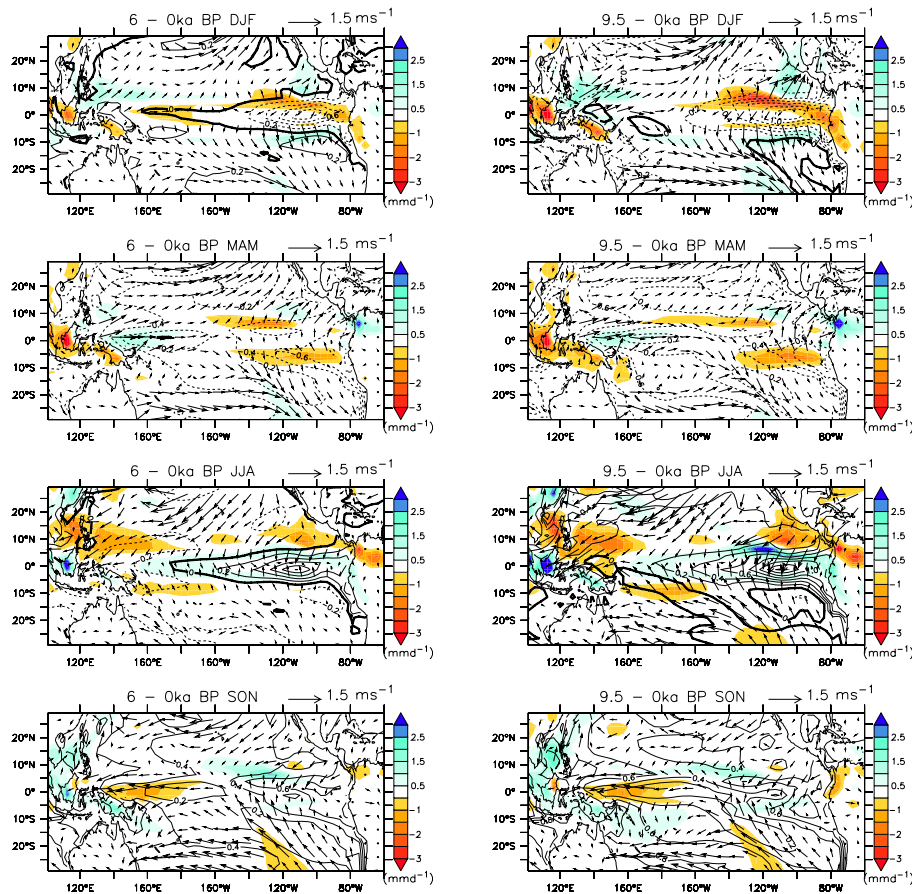


Fig. 9. Changes in simulated SST (line, °C), precipitation (color, mm d⁻¹) and wind stress anomalies (arrow, m s⁻¹) seasonal cycle for the mid-Holocene (6–0 ka, left panels) and the early Holocene (9.5–0 ka, right panels).

Early and Mid-Holocene climate in the tropical Pacific

Y. Luan et al.

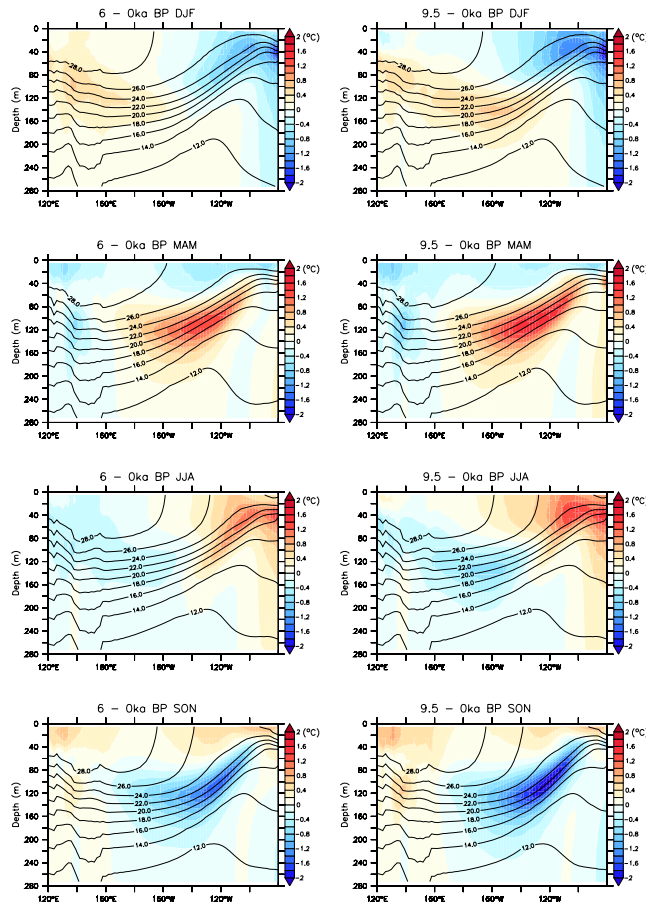


Fig. 10. Changes of the subsurface ocean temperature (color, °C) along the equator for the mid-Holocene (6–0 ka, left panels) and the early Holocene (9.5–0 ka, right panels). The equatorial sections are averaged over the 5° S and 5° N latitude band. Contour line is subsurface ocean temperature in the PI simulation.

Title Page

Abstract

Introduction

Conclusions

References

Tables

Figures

◀

▶

◀

▶

Back

Close

Full Screen / Esc

Printer-friendly Version

Interactive Discussion



Early and Mid-Holocene climate in the tropical Pacific

Y. Luan et al.

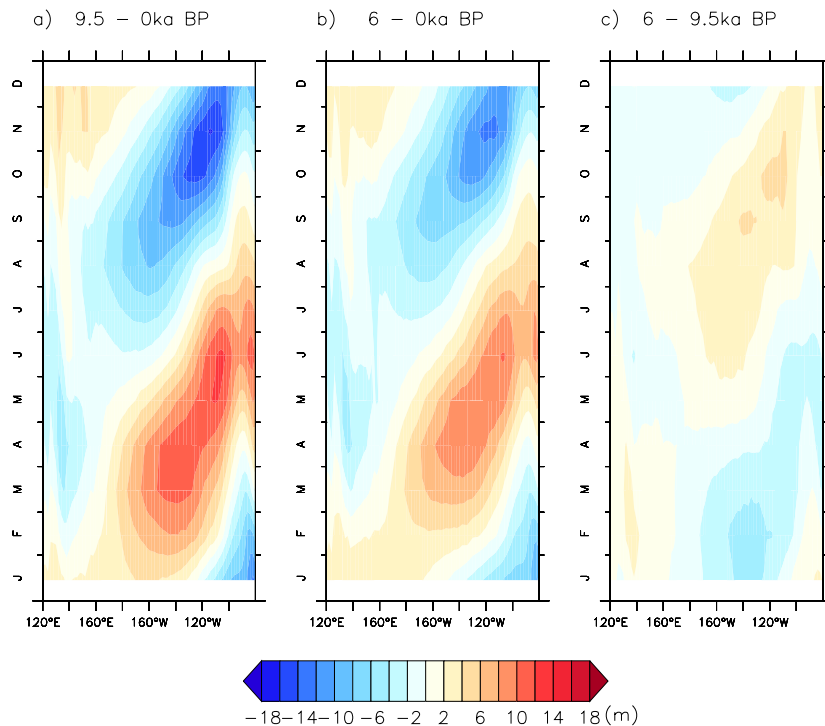


Fig. 11. Seasonal cycle of the thermocline depth as defined by the 20 °C isotherm depth (m) average between 5° S and 5° N and plotted as a function of longitude and months for **(a)** 9.5–0 ka, **(b)** 6–0 ka, **(c)** 6–9.5 ka.

Title Page

Abstract

Introduction

Conclusions

References

Tables

Figures

◀

▶

◀

▶

Back

Close

Full Screen / Esc

Printer-friendly Version

Interactive Discussion



Early and Mid-Holocene climate in the tropical Pacific

Y. Luan et al.

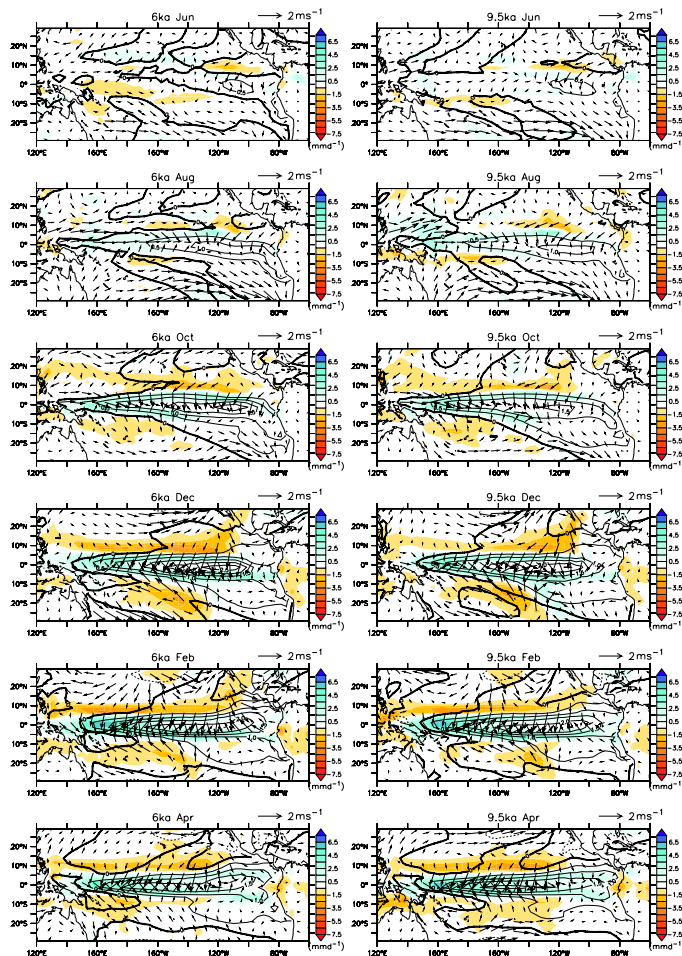


Fig. 12. Same as Fig. 2, but for the composite El Niño year in the 6 ka and 9.5 ka simulations.

Title Page

Abstract

Introduction

Conclusions

References

Tables

Figures

⏪

⏩

◀

▶

Back

Close

Full Screen / Esc

Printer-friendly Version

Interactive Discussion

Early and Mid-Holocene climate in the tropical Pacific

Y. Luan et al.

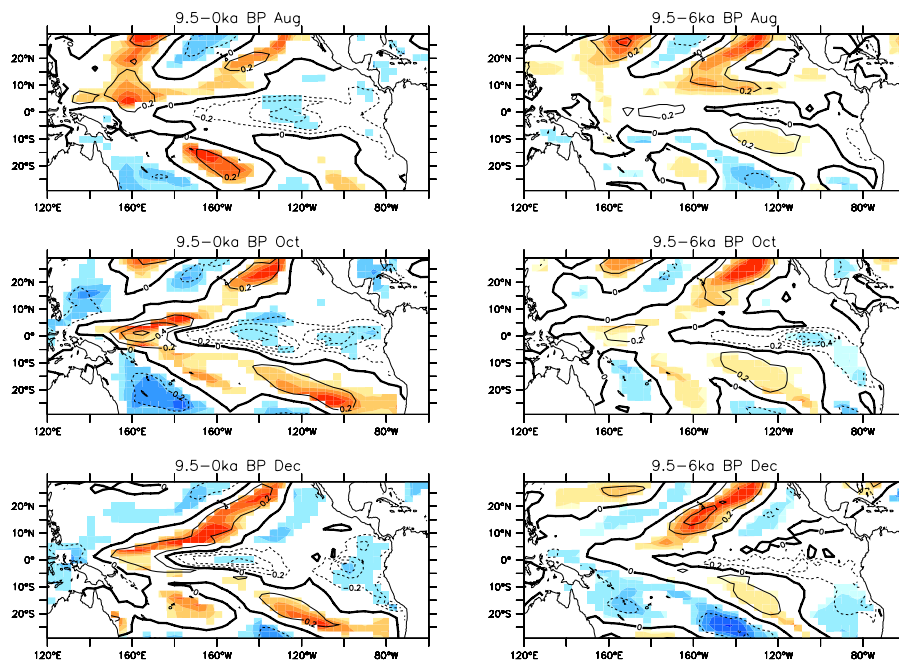


Fig. 13. Differences in SST (line, °C) during composite El Niño year between 9.5 ka and 0 ka (left panels) and 9.5 ka and 6 ka (right panels) highlighting the regions where they are significant from student T-tests.

Title Page

Abstract

Introduction

Conclusions

References

Tables

Figures

◀

▶

◀

▶

Back

Close

Full Screen / Esc

Printer-friendly Version

Interactive Discussion



Early and Mid-Holocene climate in the tropical Pacific

Y. Luan et al.

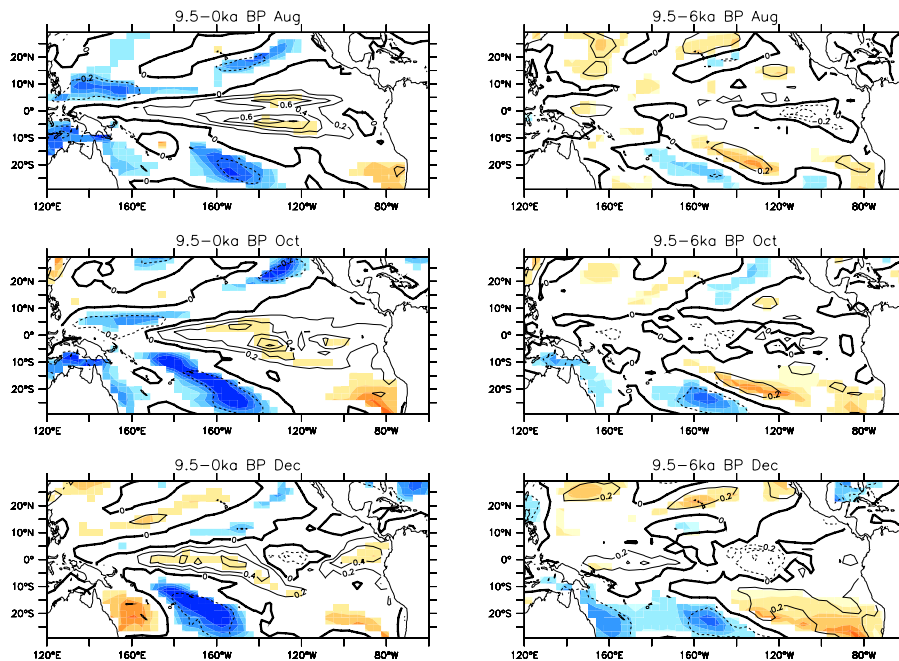


Fig. 14. Same as Fig. 13, but during composite La Niña year.

Title Page

Abstract

Introduction

Conclusions

References

Tables

Figures

◀

▶

◀

▶

Back

Close

Full Screen / Esc

Printer-friendly Version

Interactive Discussion



**Early and
Mid-Holocene climate
in the tropical Pacific**

Y. Luan et al.

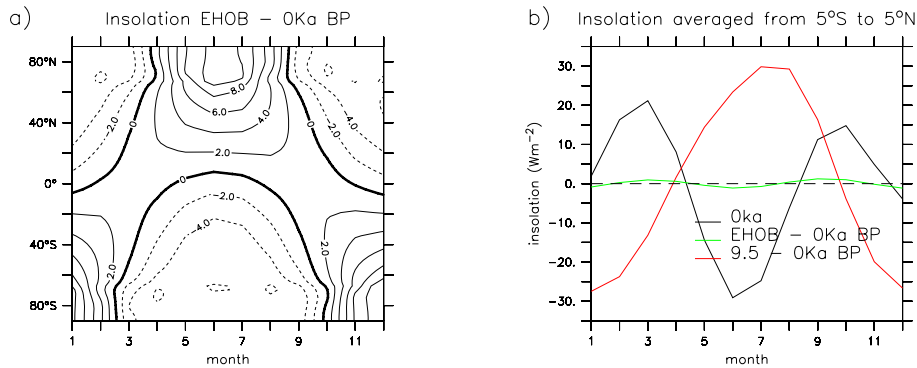


Fig. 15. Same as Fig. 3, but for the EHOB simulation.

Title Page

Abstract Introduction

Conclusions References

Tables Figures

◀ ▶

◀ ▶

Back Close

Full Screen / Esc

Printer-friendly Version

Interactive Discussion



Early and
Mid-Holocene climate
in the tropical Pacific

Y. Luan et al.

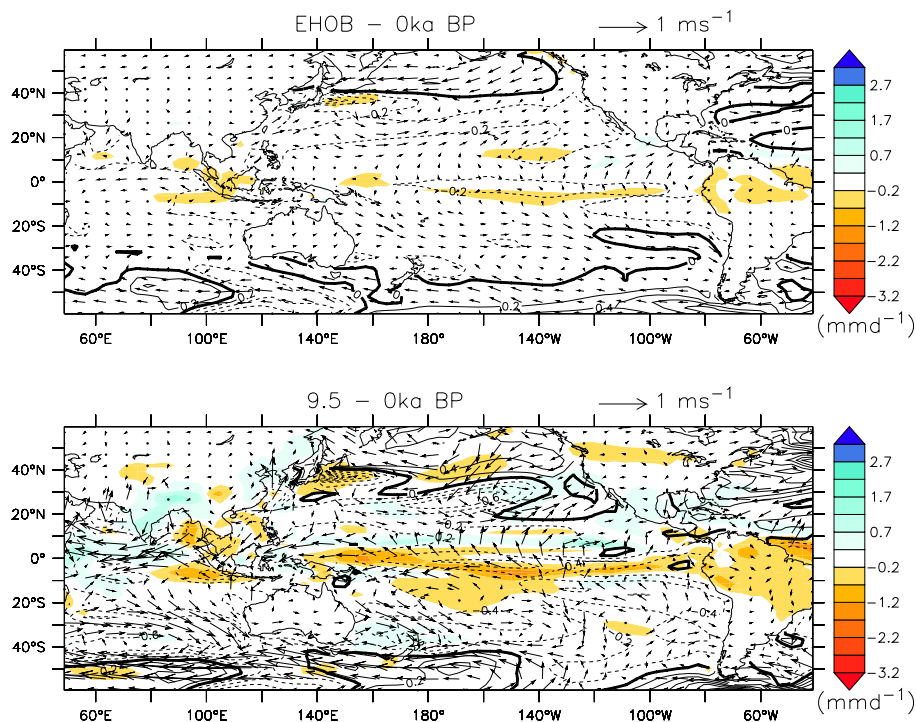


Fig. 16. Differences of annual mean SST (line, $^{\circ}\text{C}$), precipitation (color, mmd^{-1}) and wind stress anomalies (arrow, ms^{-1}) over the Pacific and Indian Oceans for **(a)** EHOB – 0 ka BP, **(b)** 9.5–0 ka BP.

[Title Page](#)[Abstract](#)[Introduction](#)[Conclusions](#)[References](#)[Tables](#)[Figures](#)[◀](#)[▶](#)[◀](#)[▶](#)[Back](#)[Close](#)[Full Screen / Esc](#)[Printer-friendly Version](#)[Interactive Discussion](#)

Early and Mid-Holocene climate in the tropical Pacific

Y. Luan et al.

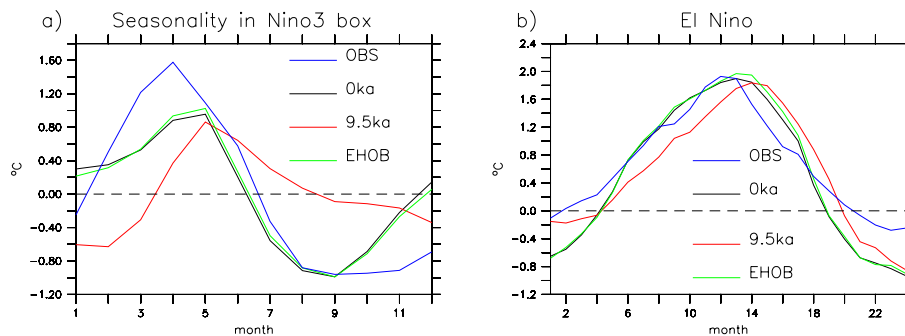


Fig. 17. Evolution of SST ($^{\circ}$ C) seasonal cycle and composites of El Niño events in Niño3 box for the different simulations.

Title Page

Abstract

Introduction

Conclusions

References

Tables

Figures

⏪

⏩

◀

▶

Back

Close

Full Screen / Esc

Printer-friendly Version

Interactive Discussion

